VESTFOLD UNIVERSITY COLLEGE
Faculty of Science and Engineering

IMST
INSTITUTT FOR MIKROSYSTEM TEKNOLOGI

MASTER THESIS

Thermoelastic influence on the performance of Film Bulk Acoustic wave Resonators

William Strømsvold

Horten, January 2009

Submitted to the Faculty of Science and Engineering, Vestfold University College, in partial fulfilment of the requirements for the degree Master of Microsystem Technology.

Abstract

Film Bulk Acoustic wave Resonators (FBAR's) are a promising new technology for high performance resonators in the GHz-range. FBAR's can provide higher Q-factors and higher coupling efficency than the typical high performance resonators, such as SAW-resonators and similar technologies.

To achieve the highest possible performance for these devices, the losses needs to be minimalized. At such high frequencies, the loss effects can have a huge influence on the total performance, and it is very useful to gain better knowledge about these loss effects.

This thesis' main goal is to investigate the thermoelastic loss effects in the metal contacts on the FBAR structure. Due to this metallization of the FBAR's, thermal losses can occur in the metal layer which can cause a degrading of the performance. An analytical model will be developed for both thermal and non-thermal influence. The model will then be realized in Matlab, in order to quantify the performance of the FBAR with the different contact materials. The Q-factor and effective coupling factor are important parameters which will be used to compare the performance.

Due to finding an important error in the Matlab code, most of the results has proven to be wrong. Unfortunately, the lack of time at the end of the project didn't give me any chance to reproduce all the plots. Nevertheless I've done calculations on Aluminium at 5 GHz, aluminium is widely used as a contact material in RF-Mems. The correct results will be shown at the presentation of the thesis.

Acknowledgements

I would like to thank my advisor, Einar Halvorsen, for always trying to answer my questions and to guide me along the way with the work of this thesis. Thanks for suggesting the subject for this thesis and providing me with excellent information about the subject.

I would like to thank Scanmar AS, for providing me with an office and computer resources to work on my thesis. Thanks to my future colleagues for being helpful and always in the mood for discussing subjects related or not related to my thesis. Scanmar also provided me with the best lunches. I am really looking forward to start working fulltime here!

And last but not least, I would also like to give my deepest appreciation to my partner, Eirin, for always being there for me.

William Strømsvold
Borre, 16. january 2009

Contents

Nomenclature

α	Linear thermal coefficient of expansion	$[m^{-1}]$
c^E_{ijkl}	Components of the second-order elastic constant tensor at constant electric field	$[Pa]$
D_i	Components of the electric displacement vector	$[N\,V^{-1}m^{-1}]$
ε^S_{ij}	Components of the dielectric permittivity constant tensor at constant strain	$[N\,V^{-2}]$
η	Entropy density	
E_i	Components of the quasi-static electric field vector	$[V\ m^{-1}]$
e_{kij}	Components of the piezoelectric strain constant	$[N\,m^{-1}V^{-1}]$
f_{ij}	Components of the thermal stress coefficient tensor	$[N\,m^{-2}K^{-1}]$
f^E_{ij}	Components of the thermal stress coefficient tensor at constant electric field	$[N\,m^{-2}K^{-1}]$
K	Bulk modulus	$[N\,m^{-2}]$
ν	Poisson ratio	$[-]$
Ω	Entropy flux	
p^S_i	Components of the pyroelectric coefficient vector at constant strain	$[N\,V^{-1}m^{-1}K^{-1}]$
ρC^E_V	Specific heat per unit volume at constant electric field	$[N\,m^{-2}K^{-1}]$
ρ	Mass density	$[kg\ m^{-3}]$

σ_s	Rate of internal entropy production per unit mass	
S_{ij}	Components of the symmetrical strain tensor	$[Pa]$
θ	Temperature increment from the steady state temperature	$[K]$
θ_0	Stress/strain free steady state temperature	$[Pa]$
T_{ij}	Components of the symmetrical stress tensor	$[Pa]$

CHAPTER 1

Introduction

1.1 Motivation

The demand for higher frequencies and higher reliability in telecommunication devices, poses huge challenges to the research being done within this field. The main goal is to design devices with higher Q-factor (Quality factor) and effective coupling, to obtain higher performance in the GHz frequency range.

A lot of research is done on Film Bulk Acoustic wave Resonators (FBAR), and it is a promising technology for integrating resonators on a silicon chip and thus providing more integrated functionality in Integrated Circuits (IC's).

To my knowledge, there hasn't been any published research on the thermoelastic losses on FBAR's. Lifshitz and Roukes [4] investigated thermoelastic damping in micro- and nanomechanical systems, with main focus on small flexural vibrations in thin beams. Prabhakar and Vengallatore [8] investigated the frequency dependence of thermoelastic damping in asymmetric, bilayered, micromechanical Euler–Bernoulli beam resonators.

The influence of the contact materials on FBAR's has gained some attention. Ueda et al. [10] did some research on finding an optimal contact material, but their results didn't include the thermal influence on the performance. Yokoyama et al. [14] did a similar study, and investigated an FBAR in FEM simulations and experiments. Both of these two studies concluded with Ruthenium being a suitable contact material for the FBAR's.

The goal for this thesis is to develop an equation set for a simple FBAR structure with metal contacts, by including the thermal effects and using the equations to establish a MATLAB model to predict the performance of the device. By comparing the thermal model to a simpler model with just the piezoelectric effects, the thermal influence can be used to see what effect this contributes to the system.

1.2 Overview

This project investigates the thermal loss effects of a 3-layer FBAR resonator. The choice of different electrode materials, may have a noticeable effect on the thermal losses in the contacts, and this will be investigated.

A simplified model of the 3-layer structure is implemented in Matlab in three steps:

The resonant frequencies are calculated for a simple 3-layer structure, consisting of *Aluminium Nitride (AlN)*, sandwiched between 2 electrodes of Aluminium. These calculations will serve as an estimate and a check to see whether the further investigations is within the ballpark.

The next step is to include the piezoelectrical effects into the 3-layer structure. The system will now have a driving force, and the results will be more accurate by including the piezoelectric effect. By including the electric field in the calculations, the impedance of the FBAR can be calculated. From the impedance of the FBAR, the quality factor and effective coupling can be calculated and we have quantitative results on the performance.

The main part of the calculations will be to include the thermal effects into the system. Both the piezoelectrical and the thermal coupling will be implemented into the equations, and the results will give us the possibility to see whether the thermal coupling will have any significant effect on the performance of the FBAR's. Several materials will be investigated, in order to see if the thermal material properties gives noticeable effects on the performance in particular.

The report will conclude with a summary of the results obtained from the simulations for both the piezoelectric and the thermopiezoelectric case.

1.3 What are Film Bulk Acoustic wave Resonators

Today wireless communication is an essential part in everyday life for most people. More and more devices gets wireless and the demand for mobile applications has never been higher. Everything is made smaller and smaller, and this puts huge demands on not only the wireless components, but on the whole systems being developed. This has led to the development of the Integrated Circuits technology which now has the ability to integrate highly complex circuits on

one single silicon chip. From the IC technology, the MEMS (Microelectromechanical Systems) technology has been developed. This allows us now to integrate, not only complex electronic circuits, but entire systems including mechanical, biological, optical functionality and many others on the same silicon chip.

With the huge growth of more and more wireless communication, the demand for the filters with higher performance to shield the receivers from noise and interference from adjacent channels is much higher. Traditionally, the high performance has been realized using SAW-technology (Surface Acoustic Wave technology), which is not compatible with the standard IC-technology.

Recently the FBAR's (Film Bulk Acoustic Resonator) has gained popularity within the research field. These devices allows for even higher performance and are compatible with the IC-process allowing for integrating a whole transmitter/receiver on one silicon chip.

FBAR's are in principal a simple structure, consisting of a piezoelectric material sandwiched between two metal layers. The performance of the FBAR is very sensitive to the physical dimensions of the structure, which demands a high precision when creating the layered structure. The FBAR's utilize the resonance properties of the piezoelectrical material, and the contact layers are just for creating contact and making it possible to apply an electric field to the FBAR in order to drive it. The contacts are usually neglected in analyzing FBAR devices, but at such a small scale the contacts can provide a loading to the system and thus providing losses and degrading of performance.

CHAPTER 2

Elastic waves in FBAR-structure

When investigating problems of this nature, it is important to make a qualified assumption of the characteristic sizes involved. For this structure, the first problem is to find approximate structural dimensions for getting resonance frequencies within the wanted range. The calculations must be simple, on a relatively simple structure, to be able to perform quick calculations.

2.1 FBAR-structure

The structure which is going to be investigated is a threelayer FBAR structure, which consists of a piezoelectric material, *AlN*, sandwiched between two identical metal layers. The dimensions of the structure are given in *Table 2.1*.

Table 2.1: Dimensions of the FBAR-structure

t_{metal}	0.1 μm
t_{piezo}	0.8 μm

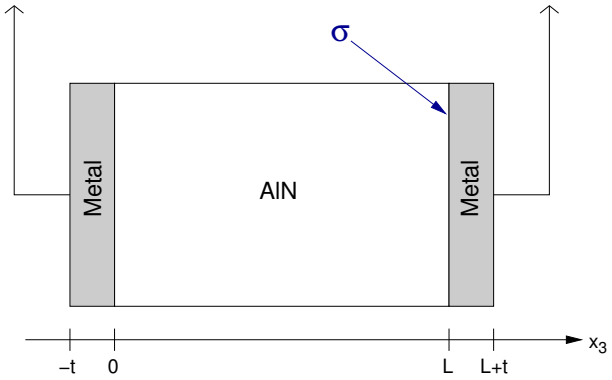

Figure 2.1: FBAR structure with the dimensions used in calculations

The piezoelectric layer is treated as a pure elastic layer with no electric effects involved. This simplifies the calculations, and gives us a quick estimate of the resonance frequencies. Timeharmonic behaviour is assumed and a plane wave solution is used for describing the wave motion within each layer. The boundary conditions connects these solutions throughout the whole structure and ensures a valid solution for the whole structure.

2.2 Mechanical equations

A cartesian coordinate system is used $O(x_1, x_2, x_3)$, and the problem is solved as a one dimensional problem with movements only in the x_3-direction.

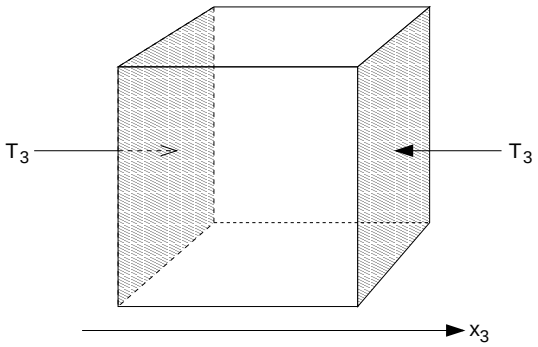

Figure 2.2: Force balance for a simple solid

To be able to describe the wave motion through the solid, we need to relate the acceleration of the particles to the forces acting through the volume. In the one-dimensional case, we can consider a slab with cross section $dA = dx_1\ dx_2$, with a net force in the x_3-direction. The net force is the

difference between the two opposing forces in the x_3-direction. Using Newton's 2nd law, we get

$$\underbrace{\frac{\partial T}{\partial x_3} dx_3 \, A}_{dF} = \underbrace{\rho A \, dx_3}_{m} \underbrace{\frac{\partial^2 u}{\partial t^2}}_{a}$$

which is simplified to

$$\frac{\partial T}{\partial x_3} = \rho \frac{\partial^2 u}{\partial t^2} \tag{2.2.1}$$

Hooke's law in one dimension describes the relation between stress, T, and strain, S

$$T_{ij} = c_{ijkl} S_{kl} \tag{2.2.2}$$

where c is the elastic stiffness tensor. Strain is defined as $S = \frac{\partial u}{\partial x_3}$, and when combining with (2.2.2) into (2.2.1) we get the one-dimensional wave equation.

$$\frac{\partial^2 u}{\partial x_3^2} = \frac{\rho}{c} \frac{\partial^2 u}{\partial t^2} \tag{2.2.3}$$

For the threelayer structure, we will use a timeharmonic wave and use a plane wave solution to solve the problem within each layer. The timeharmonic wave is given by the phasor

$$U_n = A_n e^{-ik_n x} + B_n e^{ik_n x} \qquad \text{where } k_n = \frac{\omega}{c_n} \tag{2.2.4}$$

where ω is the angular frequency and v_L is the longitudinal speed of sound which is given by

$$v_L = \sqrt{\frac{c}{\rho}}$$

2.3 Boundary conditions

The FBAR-structure will be modelled as a free structure with continuity of displacement across the internal boundaries. The free condition is fulfilled by requiring zero stress at the ends of the structure.

The boundary conditions will be used to join the solutions in each layer and get a physical solution for the whole structure.

Continuity of displacement across the internal boundaries The continuity of displacement is fulfilled by requiring equal displacement across the internal boundaries.

$$\begin{aligned} U_1|_{x=0^-} &= U_2|_{x=0^+} \\ U_2|_{x=L^-} &= U_3|_{x=L^+} \end{aligned} \tag{2.3.1}$$

This ensures that there is no relative movement between the layers.

Continuity of stress across the internal boundaries The continuity of stress is fulfilled by requiring equal stress across the internal boundaries.

$$\begin{aligned} E_1 U_1'|_{x_3=0^-} &= E_1 U_2'|_{x_3=0^+} \\ E_2 U_2'|_{x_3=L^-} &= E_3 U_3'|_{x_3=L^+} \end{aligned} \tag{2.3.2}$$

where $U_n' = \frac{\partial U_n}{\partial x_3}$.

Free ends Free end boundary conditions are

$$\begin{aligned} U_1'|_{x_3=-t} &= 0 \\ U_3'|_{x_3=L+t} &= 0 \end{aligned} \tag{2.3.3}$$

and by requiring free ends, no transmission of waves occurs at the ends and we have total reflection.

2.4 Applying the boundary conditions

The time-harmonic wave (2.2.4) is substituted into the boundary conditions, (2.3.1), (2.3.2) and (2.3.3). This gives 6 equations, which must be solved simultaneously to find the exact values for the A_n and B_n coefficients.

Continuity of displacement Applying (2.2.4) to (2.3.1) gives the following two equations:

$$A_1 + B_1 - A_2 - B_2 = 0 \tag{2.4.1}$$

$$A_2 e^{-\frac{i}{c_2}L\omega} + B_2 e^{\frac{i}{c_2}L\omega} - A_3 e^{-\frac{i}{c_3}L\omega} - B_3 e^{\frac{i}{c_3}L\omega} = 0 \tag{2.4.2}$$

Continuity of stress Applying (2.2.4) to (2.3.2) gives the following two equations:

$$-A_1 E_1 \frac{i}{c_1}\omega + B_1 E_1 \frac{i}{c_1}\omega + A_2 E_2 \frac{i}{c_2}\omega - B_2 E_2 \frac{i}{c_2}\omega = 0 \tag{2.4.3}$$

$$-A_2 E_2 \frac{i}{c_2}\omega e^{-\frac{i}{c_2}L\omega} + B_2 E_2 \frac{i}{c_2}\omega e^{\frac{i}{c_2}L\omega} + A_3 E_3 \frac{i}{c_3}\omega e^{-\frac{i}{c_3}L\omega} - B_3 E_3 \frac{i}{c_3}\omega e^{\frac{i}{c_3}L\omega} = 0 \tag{2.4.4}$$

Free ends Applying (2.2.4) to (2.3.2) gives the following two equations:

$$-A_1\frac{i}{c_1}\omega e^{\frac{i}{c_1}t\omega}+B_1\frac{i}{c_1}\omega e^{-\frac{i}{c_1}t\omega}=0 \tag{2.4.5}$$

$$-A_3\frac{i}{c_3}\omega e^{-\frac{i}{c_3}(L+t)\omega}+B_3\frac{i}{c_3}\omega e^{\frac{i}{c_3}(L+t)\omega}=0 \tag{2.4.6}$$

2.5 Matrix equation

The equations (2.4.1-2.4.6) are collected in a matrix system, $\mathbf{K}(\omega)\mathbf{A}=0$, where $\mathbf{A}$ is a column-vector with the unknown coefficient, A_n and B_n. To find the unknown coefficents, the nullspace of the K-matrix must be found.

$$\mathbf{K}(\omega)=\begin{bmatrix} 1 & 1 & -1 & -1 & 0 & 0 \\ 0 & 0 & e^{-\frac{i}{c_2}L\omega} & e^{\frac{i}{c_2}L\omega} & -e^{-\frac{i}{c_3}L\omega} & -e^{\frac{i}{c_3}L\omega} \\ -E_1\frac{i}{c_1}\omega & E_1\frac{i}{c_1}\omega & E_2\frac{i}{c_2}\omega & -E_2\frac{i}{c_2}\omega & 0 & 0 \\ 0 & 0 & -E_2\frac{i}{c_2}\omega e^{-\frac{i}{c_2}L\omega} & E_2\frac{i}{c_2}\omega e^{\frac{i}{c_2}L\omega} & E_3\frac{i}{c_3}\omega e^{-\frac{i}{c_3}L\omega} & -E_3\frac{i}{c_3}\omega e^{\frac{i}{c_3}L\omega} \\ -\frac{i}{c_1}\omega e^{\frac{i}{c_1}t\omega} & \frac{i}{c_1}\omega e^{-\frac{i}{c_1}t\omega} & 0 & 0 & 0 & 0 \\ 0 & 0 & 0 & 0 & -\frac{i}{c_3}\omega e^{-\frac{i}{c_3}(L+t)\omega} & \frac{i}{c_3}\omega e^{\frac{i}{c_3}(L+t)\omega} \end{bmatrix} \tag{2.5.1}$$

The matrix $\mathbf{K}$ is iterated over a range of ω. The inverse condition number is calculated for each ω, and the result is plotted. The inverse condition number is defined as the ratio of the smallest singular value to the largest singular value. When the inverse condition number is 0, the $\mathbf{K}$-matrix is singular.

The zero-points of the inverse condition number plot is the resonance frequencies, the frequencies where $\mathbf{K}$ is singular, thus satisfying all the boundary conditions.

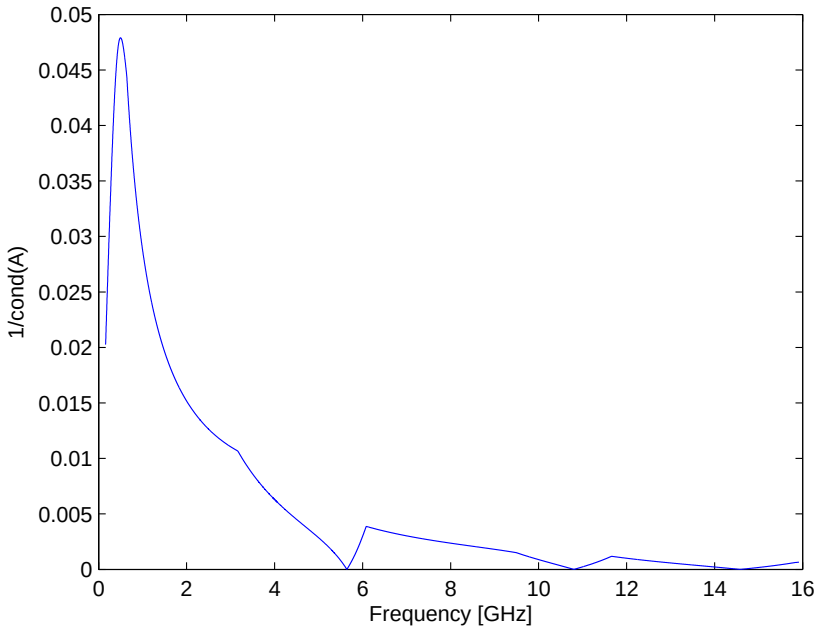

Figure 2.3: Threelayer FBAR structure with AlN piezoelectric and Al-contacts

Figure 2.3 shows the inverse condition number plot. The zero values on the plot indicates the resonance frequencies, and gives us a quick estimate of the resonance frequencies of the system. The first resonance is $\approx 5\ GHz$ which is one of the frequencies this project will investigate.

2.6 Finding exact resonance frequencies numerically

It is interesting to plot the field quantities throughout the structure, to see whether our model gives a realistic result and the boundary conditions are fulfilled correctly. The stress field is sensible to choose, since this is the effect which responds to the electric field when piezoelectric effects are introduced. To be able to plot the stress at the resonance frequencies, the exact resonance frequency must be found to make sure that the boundary conditions are fulfilled.

To find the exact resonance frequencies, we are interested in the singular case where $K(\omega)A = 0$. Assuming $K(\omega)$ is close to singular, we do a Taylor Series expansion around ω_n, the resonance frequency. For ω close to ω_n

$$K(\omega) = K(\omega_n + \{\omega - \omega_n\}) \approx K(\omega_n) + K'(\omega_n)(\omega - \omega_n) \tag{2.6.1}$$

where the bracketed term is very small and $K'(\omega_n) = \frac{\partial K(\omega_n)}{\partial \omega_n}$. Approximately we shall find

$$\begin{aligned} K(\omega_n)A + (\omega - \omega_n)K'(\omega_n)A = 0 \\ K(\omega_n)A = \mu_n K'(\omega_n)A \end{aligned} \tag{2.6.2}$$

where $\mu_n = -(\omega - \omega_n)$. (2.6.2) is on the same form as a generalized eigenvalue problem.

Generalized eigenvalue problem - Given A and B, find x and μ such that $Ax = \mu Bx$

The algorithm for refining the guess can be stated as follows

$$\begin{aligned} -(\omega_{n+1} - \omega_n) &= \mu_n \\ \omega_{n+1} &= \omega_n - \mu_n \end{aligned} \tag{2.6.3}$$

where a new frequency is found until it is sufficiently close to the resonance frequency.

2.6.1 Implementing in Matlab

The Matlab script prompts for a frequency value which is close to singular. This can be seen on the plot (*Figure 2.3*), and an approximate frequency is picked. The generalized eigenvalue problem is computed and results in a vector containing the generalized eigenvalues. The position and the smallest, absolute, real value of the eigenvalues is stored in a vector. This process is iterated until the solution converges to a constant value.

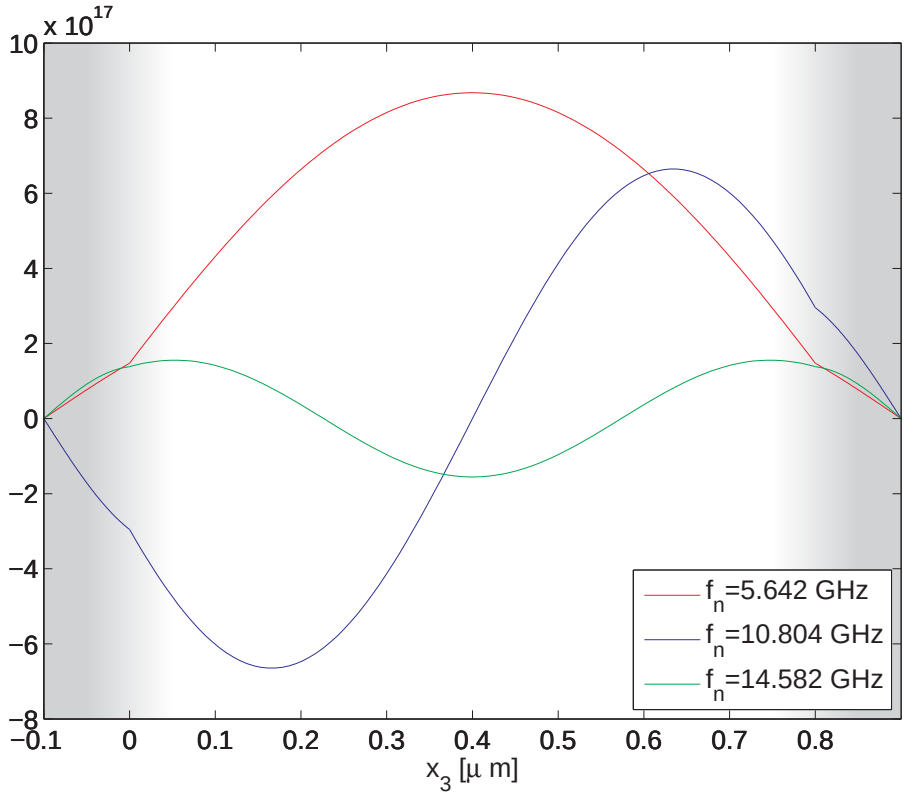

Figure 2.4: Stress through the structure at resonance frequencies

Figure 2.4 shows the stress for the three first resonance frequencies through the structure. We can see that the stress is continuous across the internal boundaries, thus fulfilling the boundary conditions.

CHAPTER 3

Piezoelectric effects in FBAR structure

The previous model was a purely elastic structure. When introducing the pioezoelectric effects, we will get the actual FBAR-structure. This model is highly idealized, considering only longitudinal vibrations in a lossless situation. This will serve as a reference to the later calculations on thermal effects which will include losses. By including the electric field in the calculations, the impedance of the structure can be found which makes it possible to quantify the performance.

3.1 Piezoelectricity

In the theory of elastic waves in solids, there are two basic field equations relating the stress/strain to the displacement. The *strain-displacement relation*

$$\mathbf{S} = \nabla_s \mathbf{u} \tag{3.1.1}$$

where $\nabla_s u_i = \frac{\partial u_j}{\partial x_i}$ is the symmetric part of the displacement gradient, and the *equation of motion*

$$\nabla \cdot \mathbf{T} = \rho \frac{\partial^2 \mathbf{u}}{\partial t^2} - \mathbf{F} \tag{3.1.2}$$

where $\mathbf{F}$ is external body force. The stress and strain are connected by the *elastic constitutive equation*

$$\mathbf{T} = \mathbf{c} : \mathbf{S} + \zeta : \frac{\partial S}{\partial t} \tag{3.1.3}$$

where ζ is the viscosity tensor and $\mathbf{F}$ is an external body force which will not be considered. The viscosity term is usually neglected, and (3.1.3) is then usually called Hooke's law and relates the stress within a material to the applied strain. This is sufficient for most materials, but some materials become electrically polarized under strain. This electric polarization causes bound electrical charges on the surface of the material [3]. These materials are called piezoelectric materials, and the phenomena is called *direct piezoelectrical effect*. This is usually linearized, by neglecting higher order effects like the electrostrictive effect for example.The polarization changes sign when the strain is reversed. There is also a reverse effect, which happens when a piezoelectric material is placed within an electric field and becomes strained. This is called the *converse piezoelectric effect*.

Piezo is derived form the greek word meaning *to press* and piezoelectricity thus means *pressure electricity*[5]. The piezoelectric materials are insulating solids, which means that when having electrodes on to adjacent surfaces, the device can act as a capacitor. When electricity is applied to the electrodes, the piezoelectric material changes shape. By applying an AC voltage, the piezoelectric crystal will start vibrating according to the frequency of the AC signal, and we then have a motor. In order to describe this phenomenon, the properties must then include a piezoelectric constant relating the electric field to the mechanical displacement in addition to the dielectric and elastic constants.

For a crystal to have piezoelectric properties, it must possess no centre of symmetry. When a crystal has no centre of symmetry, no uniform pressure can cause a separation of the center of gravity of positive and negative charges and produce an induced dipole moment which is necessary for the piezoelectric effect.

When a stress is induced on a crystal with no center of symmetry, an electric moment is developed whose magnitude is proportional to the applied stress. The magnitude of the electric moment or the polarization charge per unit area is

$$P_i = d_{ijk}\sigma_{jk} \tag{3.1.4}$$

where d_{ijk} is the piezoelectric strain constant[7]. d_{ijk} is a third rank tensor with 27 components. Practically this means if the shape of the piezoelectric crystal is being changed, an electrical field is developed within the crystal.

The piezoelectric strain constant is defined with stress as the independent variable, and measures the strain in a free crystal for a given applied field. In this work, the strain is the independent variable and hence the piezoelectric stress constant, e_{ijk} will be used, which measures the stress developed by a given field when the crystal is clamped [5]. They are related by

$$e_{nj} = d_{ni}c_{ij}^{E} \tag{3.1.5}$$

The choice of the piezoelectric constants depends on the choice of independent and dependent variables, which relates to each other through the piezoelectric constitutive equations.

3.2 Piezoelectric relations

The piezoelectric relations are coupled equations which relates the elastic and electric domain. They are derived using a thermodynamic potential based on the choice of dependent and independent variables.

We want to express the piezoelectric relations with S_{ij} and E_i as the independent variables, and and T_{ij} and D_i as the dependent variables. The first law of thermodynamics for a piezoelectric medium is given by [5].

$$dU = T_{ij}\, dS_{ij} + E_i\, dD_i \tag{3.2.1}$$

The most suitable thermodynamic potential, for our choice of variables, will be the electric enthalpy [5]

$$H = U - E_i D_i \tag{3.2.2}$$

By differentiating the electric enthalpy and substituting for dU we get

$$dH = T_{ij}\, dS_{ij} - D_i\, dE_i \tag{3.2.3}$$

which gives the following relations

$$T_{ij} = \frac{\partial H}{\partial S_{ij}} \qquad D_i = -\frac{\partial H}{\partial E_i} \tag{3.2.4}$$

We have the quadratic form of the electric enthalpy[9]

$$H = \frac{1}{2} c^E_{ijkl} S_{ij} S_{kl} - e_{ijk} E_i S_{jk} - \frac{1}{2} \varepsilon^S_{ij} E_i E_j \tag{3.2.5}$$

Using (3.2.4) on (3.2.5), we obtain the piezoelectric relations

$$T_{ij} = c^E_{ijkl} S_{kl} - e_{kij} E_k \tag{3.2.6}$$

$$D_i = e_{ikl} S_{kl} + \varepsilon^S_{ik} E_k \tag{3.2.7}$$

where

$$\begin{aligned} c_{ijkl} &= c_{ijlk} = c_{jikl} = c_{klij} \\ e_{ijk} &= e_{ikj} \\ \varepsilon_{ij} &= \varepsilon_{ji} \end{aligned} \tag{3.2.8}$$

c_{ijkl} is a fourth order tensor with $3^4 = 81$ components, which is difficult to represent in equations. Due to the symmetry in the first two and last two suffixes, it is possible to represent it as a matrix. To do this, the first two and the last two suffixes are abbreviated into a single abbreviation running from 1 to 6, as shown in *Table 3.1*.

Table 3.1: Matrix notation

ij or kl	p or q
11	1
22	2
33	3
23 or 32	4
31 or 13	5
12 or 21	6

Using the matrix notation, the governing equations for a piezoelectric material can now be written as

$$T_p = c^E_{pq} S_q - e_{kp} E_k \tag{3.2.9}$$

$$D_i = e_{iq} S_q + \varepsilon^S_{ik} E_k \tag{3.2.10}$$

where

$$S_{ij} = S_p \qquad \text{when } i = j, p = 1,2,3 \tag{3.2.11}$$

$$2S_{ij} = S_p \qquad \text{when } i \neq j, p = 4,5,6 \tag{3.2.12}$$

Using this method, the elastic, piezoelectric and dielectric constants can be written as matrices.

$$c^E_{pq} = \begin{bmatrix} c_{11} & c_{12} & c_{13} & c_{14} & c_{15} & c_{16} \\ c_{12} & c_{22} & c_{23} & c_{24} & c_{25} & c_{26} \\ c_{13} & c_{23} & c_{33} & c_{34} & c_{35} & c_{36} \\ c_{14} & c_{24} & c_{34} & c_{44} & c_{45} & c_{46} \\ c_{15} & c_{25} & c_{35} & c_{45} & c_{55} & c_{56} \\ c_{16} & c_{26} & c_{36} & c_{46} & c_{56} & c_{66} \end{bmatrix} \tag{3.2.13}$$

$$e_{ip} = \begin{bmatrix} e_{11} & e_{12} & e_{13} & e_{14} & e_{15} & e_{16} \\ e_{21} & e_{22} & e_{23} & e_{24} & e_{25} & e_{26} \\ e_{31} & e_{32} & e_{33} & e_{34} & e_{35} & e_{36} \end{bmatrix} \tag{3.2.14}$$

$$\varepsilon^S_{ij} = \begin{bmatrix} \varepsilon_{11} & \varepsilon_{12} & \varepsilon_{13} \\ \varepsilon_{12} & \varepsilon_{22} & \varepsilon_{23} \\ \varepsilon_{31} & \varepsilon_{32} & \varepsilon_{33} \end{bmatrix} \tag{3.2.15}$$

3.3 Aluminium Nitride, AlN

There are many material choices for the piezoelectric layer, but Aluminium Nitride, AlN, and Zinc Oxide, ZnO, are commonly used for FBAR resonators [11]. AlN has several advantages

over ZnO, with a higher acoustic velocity, higher Q value and a moderate electromechanical coupling factor. AlN also has a higher flexibility for depositing on different kinds of materials and substrates with excellent crystallinity [11].

The important material parameters for *AlN* are

Table 3.2: Material properties for*AlN*[2]

Property	*AlN*	Unit
ρ	3230	$[kg\ m^{-3}]$
p_3	6×10^{-6}	$[C\ m^{-2}K^{-1}]$
ε_3^S	9.5×10^{-11}	$[F\ m^{-1}]$
c_{33}^E	384.3	$[GPa]$
e_{33}	1.55	$[C\ m^{-2}]$
κ_3	285	$[W\ m^{-1}K^{-1}]$
C_V	425.387	$[J\ kg^{-1}K^{-1}]$
K	210	$[GPa]$
α	5.4×10^{-6}	$[K^{-1}]$
ν	0.245	$[-]$

The material symmetry of AlN is hexagonal in class $C_{6v} = 6mm$. This crystal class has $5+3+2=10$ independent material constants, and the material matrices are reduced to the following form [9]

$$c_{pq}^E = \begin{bmatrix} c_{11} & c_{12} & c_{13} & & & \\ c_{12} & c_{11} & c_{13} & & & \\ c_{13} & c_{13} & c_{33} & & & \\ & & & c_{44} & & \\ & & & & c_{44} & \\ & & & & & c_{66} \end{bmatrix} \tag{3.3.1}$$

where $c_{66} = \frac{1}{2}(c_{11} - c_{12})$. The piezoelectric stress constant is given by

$$e_{ip} = \begin{bmatrix} & & & & e_{15} & \\ & & & e_{15} & & \\ e_{31} & e_{31} & e_{33} & & & \end{bmatrix} \tag{3.3.2}$$

and the dielectric permittivity is given by

$$\varepsilon_{ij}^S = \begin{bmatrix} \varepsilon_{11}^S & & \\ & \varepsilon_{11}^S & \\ & & \varepsilon_{33}^S \end{bmatrix} \tag{3.3.3}$$

3.4 Three-layer structure

The constitutive equations has been developed, but they are still in tensor form and needs to be reduced to a simpler form to suit the constraints of our problem.

3.4.1 Simplification of the piezoelectric relations

In this structure, we assume:

- Plane waves in x_3-direction
- Infinite cross-section
- Displacement U only in x_3-direction. This assumption holds for special symmetry directions.
- Translation invariance within the plane

The piezoelectric material used is Aluminium Nitride AlN, which has crystal symmetry class $6mm$. The elastic stiffness tensor is given by:

$$c^E = \begin{bmatrix} c_{11}^E & c_{12}^E & c_{13}^E & & & \\ c_{12}^E & c_{11}^E & c_{13}^E & & & \\ c_{31}^E & c_{31}^E & c_{33}^E & & & \\ & & & c_{44}^E & & \\ & & & & c_{44}^E & \\ & & & & & c_{11}^E - c_{12}^E \end{bmatrix} \tag{3.4.1}$$

Since we only consider strain in the x_3-direction, the strain tensor becomes:

$$S = \begin{bmatrix} 0 \\ 0 \\ S_{33} \\ 0 \\ 0 \\ 0 \end{bmatrix} \tag{3.4.2}$$

Multiplying the stress-tensor with the stiffness tensor, we get:

$$c^E S = \begin{bmatrix} C_{13}S_{33} \\ C_{13}S_{33} \\ C_{33}S_{33} \\ 0 \\ 0 \\ 0 \end{bmatrix} \tag{3.4.3}$$

The piezoelectric stress tensor for *AlN* is given by:

$$\begin{bmatrix} 0 & 0 & 0 & 0 & e_{15} & 0 \\ 0 & 0 & 0 & e_{15} & 0 & 0 \\ e_{31} & e_{31} & e_{33} & 0 & 0 & 0 \end{bmatrix} \tag{3.4.4}$$

Multiplying the piezoelectric stress tensor with the electric field, results in:

$$e^T E = \begin{bmatrix} 0 & 0 & e_{31} \\ 0 & 0 & e_{31} \\ 0 & 0 & e_{33} \\ 0 & e_{15} & 0 \\ e_{15} & 0 & 0 \\ 0 & 0 & 0 \end{bmatrix} \cdot \begin{bmatrix} E_1 \\ E_2 \\ E_3 \end{bmatrix} = \begin{bmatrix} e_{31}E_3 \\ e_{31}E_3 \\ e_{33}E_3 \\ e_{15}E_2 \\ e_{15}E_1 \\ 0 \end{bmatrix} \tag{3.4.5}$$

$$\begin{bmatrix} T_1 \\ T_2 \\ T_3 \\ T_4 \\ T_5 \\ T_6 \end{bmatrix} = \begin{bmatrix} C_{13}S_{33} \\ C_{13}S_{33} \\ C_{33}S_{33} \\ 0 \\ 0 \\ 0 \end{bmatrix} - \begin{bmatrix} e_{31}E_3 \\ e_{31}E_3 \\ e_{33}E_3 \\ e_{15}E_2 \\ e_{15}E_1 \\ 0 \end{bmatrix} \tag{3.4.6}$$

Newton's 2. law states that

$$\begin{aligned} -\rho\omega^2 U &= \frac{\partial T_{3(x)}}{\partial x} + \frac{\partial T_{3(y)}}{\partial y} + \frac{\partial T_{3(z)}}{\partial z} \\ &= \frac{\partial T_3}{\partial z} \end{aligned} \tag{3.4.7}$$

The dielectric permittivity tensor is

$$\begin{bmatrix} \varepsilon_{11} & \varepsilon_{12} & \varepsilon_{13} \\ 0 & \varepsilon_{11} & \varepsilon_{23} \\ 0 & 0 & \varepsilon_{33} \end{bmatrix} \tag{3.4.8}$$

The *S,E-relation* reduces to:

$$\begin{aligned} T_3 &= c_{33}^E S_3 - e_{33}E_3 \\ D &= e_{33}S_3 + \varepsilon_3^S E_3 \end{aligned} \tag{3.4.9}$$

3.5 Boundary conditions

We use the time-harmonic wave with complex amplitude

$$U_n(x) = A_n e^{-i\frac{\omega}{c_n}x} + B_n e^{i\frac{\omega}{c_n}x} \tag{3.5.1}$$

The boundaries constraining the problem are:

Continuity of displacement across internal boundaries Continuity of displacement across internal boundaries are fulfilled by requiring equal displacement across internal boundaries

$$U_3^L|_{x_3=0^-} = U_3^M|_{x_3=0^+} \tag{3.5.2}$$

$$U_3^M|_{x_3=L^-} = U_3^R|_{x_3=L^+} \tag{3.5.3}$$

This ensures no relative displacement between the layers.

Continuity of stress across internal boundaries We now have a piezoelectric layer to consider, and the stress within the piezoelectric layer is given by (3.2.9). Since we only consider strain in the x_3-direction, the govering piezoelectric relations become

$$E^L \frac{\partial U_3^L}{\partial x_3}|_{x_3=0^-} = T_3|_{x_3=0^+} \tag{3.5.4}$$

$$T_3|_{x_3=L^-} = E^R \frac{\partial U_3^R}{\partial x_3}|_{x_3=L^+} \tag{3.5.5}$$

where E^n is the stiffness constant for the contact material and the superscript indicates the layer.

$$T_3 = c_{33}^E S_3 - e_{33} E_3 \tag{3.5.6}$$

$$D = e_{33} S_3 + \varepsilon_3^S E_3 \tag{3.5.7}$$

Free ends We require free ends, which means that the stress must equal zero at the ends

$$E^L \frac{\partial U_3^L}{x_3}|_{x_3=-t} = 0 \tag{3.5.8}$$

$$E^R \frac{\partial U_3^R}{x_3}|_{x_3=L+t} = 0 \tag{3.5.9}$$

3.6 Applying the boundary conditions

3.6.1 Mechanical boundary conditions

Continuity of displacement across the internal boundaries This boundary condition as applied in the same way as done in *Section 2.4*.

Continuity of stress across the internal boundaries The dependency on the electric field removed by substituting the second equation in (3.5.7), into the first, to get

$$T_3 = c_{33}^D \frac{\partial U_3}{\partial x_3} - \frac{e_{33}}{\varepsilon_3^S} D_3 \tag{3.6.1}$$

where $c_{33}^D = c_{33}^E + \frac{e_{33}^2}{\varepsilon_3^S}$. We have the condition $D_3 = -\sigma$, which results in

$$T_3 = c_{33}^D \frac{\partial U_3}{\partial x_3} + \frac{e_{33}}{\varepsilon_3^S}\sigma \tag{3.6.2}$$

By inserting into (3.5.5) we get the equation for $x_3 = 0$

$$-E^L \frac{i}{v^L}\omega A_1 + E^L \frac{i}{v^L}\omega B_1 + c_{33}^D \frac{i}{v^M}\omega A_2 - c_{33}^D \frac{i}{v^M}\omega B_2 = \frac{e_{33}}{\varepsilon_3^S}$$

The term after the equals sign is zero at this boundary. For the interface at $x_3 = L$ we get

$$-c_{33}^D \frac{i}{v^M}\omega e^{-\frac{i}{v^M}L\omega} A_2 + c_{33}^D \frac{i}{v^M}\omega e^{\frac{i}{v^M}L\omega} B_2 + E^R \frac{i}{v^R}\omega e^{-\frac{i}{v^R}L\omega} A_3 - E^R \frac{i}{v^R}\omega e^{\frac{i}{v^R}L\omega} B_3 = -\frac{e_{33}}{\varepsilon_3^S}$$

Free ends For the free ends we get the following equations. For the location at $x_3 = -t$

$$-E^L \frac{i}{v^L}\omega e^{-\frac{i}{v^L}(-t)\omega} A_1 + E^L \frac{i}{v^L}\omega e^{\frac{i}{v^L}(-t)\omega} B_1 = -\frac{e_{33}}{\varepsilon_3^S}\sigma \tag{3.6.3}$$

and for the location at $x_3 = L + t$

$$-E^R \frac{i}{v^R}\omega e^{-\frac{i}{v^R}(L+t)\omega} A_3 + E^R \frac{i}{v^R}\omega e^{\frac{i}{v^L}(L+t)\omega} B_3 = -\frac{e_{33}}{\varepsilon_3^S}\sigma \tag{3.6.4}$$

In both of these equations, the term after the equals sign is zero because the only location σ is assigned is at $x_3 = L$.

3.6.2 Electrical boundary conditions

In order to calculate the impedance, an expression for the voltage must be found. In the FBAR structure, the charge density is defined as a constant at $x_3 = L$

$$-D_3 = \sigma \tag{3.6.5}$$

From the relation in (3.4.9) we have

$$-D_3 = \varepsilon_3^S \frac{\partial \varphi}{\partial x_3} - e_{33}\frac{\partial U_2}{\partial x_3} = \sigma \tag{3.6.6}$$

Voltage is defined as the integral of the electric field through the structure

$$V = \int_0^L \frac{\partial \varphi}{\partial x_3} dz = \varphi(L) - \varphi(0) \tag{3.6.7}$$

Integrating eqref through the piezoelectric material from $x_3 = 0$ to $x_3 = L$

$$V = \int_0^L \frac{\partial \varphi}{\partial x_3} \partial x_3 = \frac{e_{33}}{\varepsilon_3^S} \int_0^L \frac{\partial U_2}{\partial x_3} \partial x_3 + \frac{1}{\varepsilon_3^S} \int_0^L \sigma \partial x_3 \tag{3.6.8}$$

which leads to an expression for the voltage in the pizeoelectric layer

$$V = \frac{e_{33}}{\varepsilon_3^S} \{U_2(L) - U_2(0)\} + \frac{L}{\varepsilon_3^S} \sigma \tag{3.6.9}$$

Inserting the plane wave from (3.5.1) gives

$$V = \frac{e_{33}}{\varepsilon_3^S} \left(e^{-\frac{i}{c_2} L\omega} - 1 \right) A_2 + \frac{e_{33}}{\varepsilon_3^S} \left(e^{\frac{i}{c_2} L\omega} - 1 \right) B_2 + \frac{L}{\varepsilon_3^S A} Q \tag{3.6.10}$$

where $Q = \sigma A$. Identifying $\frac{\varepsilon_3^S A}{L}$ as the capacitance C_p, (3.6.10) can be expressed as.

$$V = \mathbf{TA} + \frac{1}{C_p} Q \tag{3.6.11}$$

where $\mathbf{T}$ is

$$\mathbf{T} = \begin{bmatrix} 0 & 0 & \frac{e_{33}}{\varepsilon_3^S} \left(e^{-\frac{i}{c_2} L\omega} - 1 \right) & \frac{e_{33}}{\varepsilon_3^S} \left(e^{\frac{i}{c_2} L\omega} - 1 \right) & 0 & 0 \end{bmatrix}$$

and $\mathbf{A}$ is a column vector with the unknown coefficients

$$\mathbf{A} = \begin{bmatrix} A_1 & B_1 & A_2 & B_2 & A_3 & B_3 \end{bmatrix}^T \tag{3.6.12}$$

CHAPTER 4

Thermal effects

In the previous chapter, the piezoelectric effects of a threelayer FBAR structure has been investigated.

In this chapter, thermal effects will be included to make a more realistic model of the FBAR structure. This will be done to be able to see the effects caused by the interaction between heat and the piezoelectric effects.

4.1 Loss effects

An ideal FBAR will have no energy loss and hence a very high Q value. In a realistic device the performance will be lower due to different dissipation mechanisms within the structure. The typical loss effects are shortly being introduced here, in order to understand the factors which can influence the performance of an FBAR.

4.1.1 Thermal loss

The classical thermoelastic theory was developed by Zener [15]. When stress is applied to a crystal, there will be a minor temperature change in the crystal. The temperature changes in the different parts of the crystal will cause a heat flow which tries to equalize the temperature

difference. These effects causes heat dissipation and anelastic behaviour of the crystal.

4.1.2 Structural loss

Structural losses, and especially anchor losses, are related to mechanical waves propagating into the structure surrounding the FBAR. This could typically be the clamping of the resonating structure, and the waves propagating through this and further into the substrate. Due to often more complicated geometries, these losses are typically solved using Finite Element methods.

4.1.3 Contact loss

The metal contacts on the FBAR can be a source of loss, due to the resistivity of the metal. At higher frequencies, this can lead to a substantial loss of effect in the FBAR.

4.1.4 Phonon loss

A phonon is a quantized mode of vibration in a crystal lattice, and is very important in describing many physical properties of solids, especially electrical and thermal conductivity. The incident elastic wave, which can be seen as a beam of phonons, interacts with the thermal phonons in the crystal and disturbs the thermal equilibrium. The interaction of ultrasonic waves with the lattice vibrations of a crystal, cause an irreversible process which attenuates the ultrasonic waves. The relaxation time constant for the phonon distribution is much smaller than for the thermal conduction, and this separates these two types of losses. Both thermoelastic damping and phonon losses are due to anharmonic behaviour of the crystal lattice [6, Chap. 17].

4.1.5 Morphology, crystal quality

In an ideal situation, the surface of the piezoelectric layer and the contact layer is perfectly smooth and has perfect contact. This is certainly not the case in a real device. Surface roughness and crystalline quality are important factors for the piezoelectrical material, and the compatibility with the contact material for achieving a smooth interface as possible must be considered. This can give considerable losses in the performance of the FBAR. Ueda et al. [10] investigated an $Ru/AlN/Ru$ FBAR structure, and proved that smoothing the Ruthenium layer resulted in a higher Q-value and coupling factor. They indicated that the crystalline quality of the AlN-films were primarily related to the surface roughness of the underlayers, rather than the crystalline qualities of the underlayer.

The surface quality of the contact and piezoelectric layers will not be investigated in this thesis, but can be a huge factor in the loss of FBAR's.

4.2 Pyroelectricity

Pyroelectricity is an effect which can occur in a crystal possessing no centre of symmetry [7]. A temperature change develops an electric polarization, and results in two pyroelectric effects. If the crystal is clamped, the polarization measured is the *primary* pyroelectricity. If the crystal is free to expand, both the primary and the secondary pyroelectric effect is measured. Pyroelectricity is defined as

$$\Delta P_i = p_i \Delta T \tag{4.2.1}$$

where p_i is the pyroelectric coefficient. Notice that this is a crystal property which is represented by a vector. The pyroelectric effect is not a permanent effect, but fades out due to imperfect insulation over time. The pyroelectric effect becomes neutralized due to surface migration of charges to the surface of the crystal.

4.3 Thermal stress

When introducing the thermal effects into the piezoelectric relations, depending on the choice of variables, the stress induced by temperature is called f_{ij} [7]. Due to symmetry, f_{ij} also relates the entropy/heat produced by a strain. We have the relation

$$f_{ij}^E = \frac{\partial \eta}{\partial S_{ij}}^{E,\theta} = -\frac{\partial T_{ij}}{\partial \theta} \tag{4.3.1}$$

$f_i j$ is the product of the linear thermal expansion coeffient α and the bulk modulus K

$$f_{ij} = \alpha K \tag{4.3.2}$$

where the bulk modulus is defined as

$$K = \frac{c_{ijkl}}{3(1-2\nu)} \tag{4.3.3}$$

where ν is the Poisson ratio.

4.4 Material properties for the contact materials

The material properties for the contact materials have been gathered in *Table 4.1* The relative dielectric permittivity of the metals are set to $\varepsilon_r = 1$ [16, p. 37].

Table 4.1: Material properties for the contact materials[13]

Property	**Al**	**Ru**	**Mo**	**Pt**	Unit
ρ	2700	12370	10280	21090	$[kg\ m^{-3}]$
v	5100	5970	6190	2680	$[m\ s^{-1}]$
c	70	447	329	168	$[GPa]$
K	76	220	230	230	$[GPa]$
ν	0.35	0.30	0.31	0.38	$[-]$
κ	235	120	139	72	$[W\ m^{-1}K^{-1}]$
α	23.1	6.4	4.8	8.8	$[\cdot 10^{-6}K^{-1}]$
C_V	896.91	238.053	250.782	132.558	$[J\ kg^{-1}\ K^{-1}]$

4.5 Constitutive equations

The relation between different measurable quantities of crystal defines the material properties. The relation between stress and strain defines the stiffness or compliance, the relation between the electric field and the electric displacement defines the electric permittivity and the relation between entropy and temperature defines the heat capacities. In a piezoelectric material, these relations exists between the different electrical and mechanical domains. When introducing the thermal effects into the crystal, the thermal domain relates both to the electrical and mechanical domain, and the material properties are not independent of each other. In this treatment we assume that the quantities are quasistatic and thermodynamically reversible, thus can be described by reference to an equilibrium state. The properties of the crystal are then in equilibrium with its surroundings, which means that the state of the crystal or its surroundings doesn't change with time.

To establish the constitutive relations between the different measurable quantities of a crystal, a set of independent and dependent variables must be chosen.

Dependent variables T_{ij} (stress), D_i (electric displacement) and η (entropy)

Independent variables S_{ij} (strain), E_i (electric field) and θ (temperature)

The energy of the system is consisting of a small flow of heat into the crystal and the work done on the crystal, assuming unit volume. According to the first law of thermodynamics, the increase of internal energy is a perfect differential

$$dU = dQ + dW \tag{4.5.1}$$

where dQ is a small flow of heat into the crystal and dW is the work done on the crystal. The work done by the different forces is a sum of the mechanical strain caused by stress within the crystal and the piezoelectric polarization forces

$$dW = dW_{strain} + dW_{polarization} \tag{4.5.2}$$

The work done by a small stress on the unit volume is given by

$$dW = T_{ij}\, dS_{ij} \tag{4.5.3}$$

and the work done by polarization of the crystal, when the field is being entirely confined to the crystal is, assuming unit volume,

$$dW = E_i\, dD_i \tag{4.5.4}$$

The second law of thermodynamics states that for a reversible change

$$dQ = \theta\, d\eta \tag{4.5.5}$$

where θ is the temperature and η is the entropy density. The total energy of the system then becomes

$$dU = T_{ij}\, dS_{ij} + E_i\, dD_i + \theta\, d\eta \tag{4.5.6}$$

Based on the choice of dependent and independent variables, a proper thermodynamical potential must be chosen. In this case, the electric Gibbs function is most suitable[5], since it contains E, D, η and θ

$$G = U - E_i D_i - \eta\,\theta \tag{4.5.7}$$

By differentiating the electric Gibbs function (4.5.7), and substituting for dU with (4.5.6)

$$dG = dU - E\, dD - D\, dE - \eta\, d\theta - \theta\, d\eta \tag{4.5.8}$$

we get the differential relations between the dependent and independent variables for the system

$$dG = T_{ij}\, dS_{ij} - D_i\, dE_i - \eta\, d\theta \tag{4.5.9}$$

The dependent variables can be identified from (4.5.9)

$$T_{ij} = \frac{\partial G}{\partial S_{ij}} \qquad D_i = -\frac{\partial G}{\partial E_i} \qquad \eta = -\frac{\partial G}{\partial \theta} \tag{4.5.10}$$

The quartic form of the thermodynamic potential is given by [1]

$$G = \frac{1}{2} c^{E,\theta}_{ijkl} S_{ij} S_{kl} - e^{\theta}_{ijk} E_i S_{jk} - \frac{1}{2} \varepsilon^{S,\theta}_{ij} E_i E_j - \frac{\rho C^E_V}{\theta_0} \theta^2 - p^S_i \theta E_i - f^E_{ij} S_{ij} \theta \tag{4.5.11}$$

where ρC^E_V is the specific heat per unit volume at constant electric field, θ_0 is the stress/strain free temperature, p^S_i are components of the pyroelectric coefficient vector at constant strain, f^E_{ij} are components of the thermal stress constant tensor at constant electric field. Using (4.5.10) on the quartic form of the thermodynamic potential (4.5.11) we get the final constitutive equations for the thermopiezoelectric solid

$$T_{ij} = c^{E,\theta}_{ijkl} S_{kl} - e^{\theta}_{kij} E_k - f^E_{ij} \theta \tag{4.5.12}$$

$$D_i = e^{\theta}_{ijk} S_{jk} + \varepsilon^{S,\theta}_{ij} E_j + p^S_i \theta \tag{4.5.13}$$

$$\eta = f^E_{ij} S_{ij} + p^S_i E_i + \frac{\rho C^E_V}{\theta_0} \theta \tag{4.5.14}$$

The material constants satisfy the following symmetrical conditions

$$\begin{array}{ccc} c_{ijkl} = c_{klij} = c_{jikl} = c_{ijlk} & & f_{ij} = f_{ji} \\ \kappa_{ij} = \kappa_{ji} & \varepsilon_{ij} = \varepsilon_{ji} & e_{ikl} = e_{ilk} \end{array} \tag{4.5.15}$$

4.5.1 Isothermal and adiabatic material constants

The properties of a material are usually measured statically at constant temperature. The material properties are then isothermal, which means that the variations in temperature are happening so slowly that the temperature is constant throughout the whole material and across the boundaries. For a material vibrating at a high frequency there is no chance for the temperature to equalize throughout the material, and we can say that the heat is confined within the boundaries allowing no heat to escape or enter the material. The adiabatic constants are determined at constant entropy in the system.

For gases there is a noticeable difference between the adiabatic and isothermal situation. For piezoelectric materials, this difference is smaller, and it is common to ignore this difference. Although the difference between the isothermal and adiabatic material constants will be developed in this section, in order to see whether or not they have any effect..

First the differentials are written out for the chosen variables, with respect to each component, keeping all other components constant. The superscripts indicates the components held constant.

$$dT_{ij} = \left(\frac{\partial T_{ij}}{\partial S_{kl}}\right)^{E,\theta} dS_{kl} + \left(\frac{\partial T_{ij}}{\partial E_k}\right)^{S,\theta} dE_k + \left(\frac{\partial T_{ij}}{\partial \theta}\right)^{S,E} d\theta \tag{4.5.16}$$

$$dD_i = \left(\frac{\partial D_i}{\partial S_{jk}}\right)^{E,\theta} dS_{jk} + \left(\frac{\partial D_i}{\partial E_j}\right)^{S,\theta} dE_j + \left(\frac{\partial D_i}{\partial \theta}\right)^{S,E} d\theta \tag{4.5.17}$$

$$d\eta = \left(\frac{\partial \eta}{\partial S_{ij}}\right)^{E,\theta} dS_{ij} + \left(\frac{\partial \eta}{\partial E_i}\right)^{S,\theta} dE_i + \left(\frac{\partial \eta}{\partial \theta}\right)^{S,E} d\theta \tag{4.5.18}$$

The Einstein summation conventions is used, giving 13 equations with each equation having 13 components on the right hand side. Each of the differential coefficients are material parameters "measured" under different conditions. By comparing (4.5.18) with (4.5.12)-(4.5.14), we can see the relations between the differentials and the material parameters.

$$c_{ijkl}^{E,\theta} = \left(\frac{\partial T_{ij}}{\partial S_{kl}}\right)^{E,\theta} \qquad e_{kij}^{\theta} = -\left(\frac{\partial T_{ij}}{\partial E_k}\right)^{S,\theta} \qquad \varepsilon_{ij}^{S,\theta} = \left(\frac{\partial D_i}{\partial E_j}\right)^{S,\theta} \tag{4.5.19}$$

The second equation in (4.5.19) makes no sense to be measured at constant strain, so the piezoelectric stress constant is only measured at constant temperature. According to the second law of thermodynamics, for a reversible change

$$dQ = \theta_0 d\eta \tag{4.5.20}$$

and substituting (4.5.14) into (4.5.20)

$$dQ = \theta_0 d\eta = \theta_0 f_{ij}^E \, dS_{ij} + \theta_0 p_i^S \, dE_i + \rho C_V^E \, d\theta \tag{4.5.21}$$

To find the adiabatic constants, the heat flow must be $dQ = 0$, and by setting (4.5.21) equal to zero and solving for $d\theta$, we can use it to eliminate the temperature change.

$$d\theta = -\frac{f_{ij}^E \theta_0}{\rho C_V^E} dS_{ij} - \frac{p_i^S \theta_0}{\rho C_V^E} dE_i \tag{4.5.22}$$

Adiabatic stiffness constant

c_{ijkl}^η is defined as $\left(\frac{dT_{ij}}{dS_{kl}}\right)^\eta$, and the reasonable choice for finding this constant would be to use (4.5.18), using the material coefficients from (4.5.12), and setting $dE_k = 0$ since this constant is in the thermomechanical domain. First (4.5.22) is substituted into (4.5.18) to eliminate the temperature dependence, and we have constant entropy

$$dT_{ij} = c_{ijkl}^{E,\theta} \, dS_{kl} - e_{kij}^\theta \, dE_k - f_{ij}^E \left(-\frac{f_{kl}^E \theta_0}{\rho C_V^E} dS_{kl} - \frac{p_k^S \theta_0}{\rho C_V^E} dE_k \right) \tag{4.5.23}$$

Setting $dE_k = 0$ eliminates the influence of the electric field

$$dT_{ij} = c_{ijkl}^{E,\theta} \, dS_{kl} + \frac{f_{ij}^E f_{kl}^E \theta_0}{\rho C_V^E} dS_{kl} \tag{4.5.24}$$

Identifying $c_{ijkl}^\eta = \left(\frac{dT_{ij}}{dS_{kl}}\right)^\eta$ gives us the following relation between isothermal and adiabatic stiffness

$$c_{ijkl}^\eta = c_{ijkl}^{E,\theta} + \frac{f_{ij}^E f_{kl}^E \theta_0}{\rho C_V^E} \tag{4.5.25}$$

Adiabatic piezoelectric stress constant, e_{ijk}^η

e_{ijk}^η is defined as $-\left(\frac{\partial T_{ij}}{\partial E_k}\right)_\eta$ and (4.5.12) will be used together with setting $dS_{kl} = 0$ to obtain the clamped piezoelectric stress constant. In the same way, (4.5.22) is substituted into (4.5.12) to fulfill the constant entropy condition.

$$dT_{ij} = c_{ijkl}^{E,\theta} \, dS_{kl} - e_{kij}^\theta \, dE_k - f_{ij}^E \left(-\frac{f_{kl}^E \theta_0}{\rho C_V^E} \, dS_{kl} - \frac{p_k^S \theta_0}{\rho C_V^E} \, dE_k \right) \tag{4.5.26}$$

Setting $dS_{kl} = 0$ gives

$$dT_{ij} = -e^{\theta}_{kij}\, dE_k + \frac{f^E_{ij} p^S_k \theta_0}{\rho C^E_V}\, dE_k \tag{4.5.27}$$

Identifying $e^{\eta}_{kij} = -\left(\frac{\partial T_{ij}}{\partial E_k}\right)^{\eta}$ gives us the following relation between isothermal and adiabatic piezoelectric stress constant

$$e^{\eta}_{kij} = e^{\theta}_{kij} - \frac{f^E_{ij} p^S_k \theta_0}{\rho C^E_V} \tag{4.5.28}$$

Adiabatic dielectric constant

ε^{η}_{ik} is defined as $\left(\frac{\partial D_i}{\partial E_j}\right)^{\eta}$ and (4.5.13) will be used together with $dS_{jk} = 0$ to obtain the clamped adiabatic dielectric constant. (4.5.22) is substituted into (4.5.13) to fulfill the constant entropy condition

$$dD_i = e^{\theta}_{ijk}\, dS_{jk} + \varepsilon^{S,\theta}_{ij}\, dE_j + p^S_i \left(-\frac{f^E_{jk}\theta_0}{\rho C^E_V}\, dS_{jk} - \frac{p^S_j \theta_0}{\rho C^E_V}\, dE_j \right) \tag{4.5.29}$$

Setting $dS_{jk} = 0$ gives

$$dD_i = \varepsilon^{S,\theta}_{ij}\, dE_j - \frac{p^S_i p^S_j \theta_0}{\rho C^E_V}\, dE_j \tag{4.5.30}$$

Identifying $\varepsilon^{\eta}_{ij} = \left(\frac{\partial D_i}{\partial E_j}\right)_{\eta}$ gives us the following relation between isothermal and adiabatic dielectric constant

$$\varepsilon^{\eta}_{ij} = \varepsilon^{\theta}_{ij} - \frac{p^S_i p^S_j \theta_0}{\rho C^E_V} \tag{4.5.31}$$

Influence of the adiabatic constants

Usually for solid materials, the difference between the isothermal and adiabatic material constants are neglected. The difference is small, but can still have an noticeable influence for the higher frequencies. The relative difference between the isothermal and adiabatic constants has been calculated for *AlN*

$$\frac{c^{\eta}_{ijkl}}{c^{\theta}_{ijkl}} \approx 1.001 \qquad \frac{e^{\eta}_{ijk}}{e^{\theta}_{ijk}} \approx 0.999 \qquad \frac{\varepsilon^{\eta}_{ij}}{\varepsilon^{\theta}_{ij}} \approx 0.999 \tag{4.5.32}$$

For the simulations, the adiabatic material constants will be used.

Table 4.2: Isothermal and adiabatic material constants

Parameter	Isothermal	Adiabatic
c_{33}^{E}	384.3 *GPa*	384.7 *GPa*
e_{33}^{S}	1.55 $\frac{N}{V \cdot m}$	1.5482 $\frac{N}{V \cdot m}$
ε_{3}^{S}	9.5×10^{-11} $F\ m^{-1}$	9.499×10^{-11} $F\ m^{-1}$

4.6 Developing the field equations

The following constitutive equations include thermal effects

$$T_{ij} = c_{ijkl}^{E,\theta} S_{kl} - e_{kij}^{\theta} E_k - f_{ij}^{E} \theta$$
$$D_i = e_{ijk}^{\theta} S_{jk} + \varepsilon_{ij}^{S,\theta} E_j + p_i^{S} \theta$$
$$\eta = f_{ij}^{E} S_{ij} + p_i^{S} E_i + \frac{\rho C_V^{E}}{\theta_0} \theta$$

We will use the constitutive equations including the thermal effects, to develop the field equations which will be used in the MATLAB model. To ease the notation, the upper indices will be neglected in developing the field equations.

4.6.1 Linearized mechanical equation of motion

As shown in (2.2.1), the linearized mechanical equation of motion in one dimension is given by

$$\frac{\partial}{\partial x_i}(T_{ij}) = \rho \frac{\partial^2 U_j}{\partial t^2} \tag{4.6.1}$$

Substituting (4.5.12) into (4.6.1) gives

$$\rho \frac{\partial^2 U_i}{\partial t^2} = \frac{\partial}{\partial x_i}(c_{ijkl}\ S_{kl} - e_{kij}\ E_k - f_{ij}\ \theta) \tag{4.6.2}$$

4.6.2 Linearized heat conduction equation

The entropy constitutive equation is used to derive the heat equation for the thermopiezoelectric case. Rearranging (4.5.14) and multiplying by the mass density, ρ

$$\frac{C_v}{\theta_0}\theta = \frac{\eta}{\rho} - \frac{f_{ij}}{\rho} S_{ij} - \frac{p_i}{\rho} E_i$$
$$\rho C_v \theta = \theta_0 \eta - \theta_0 f_{ij} S_{ij} - \theta_0 p_i E_i$$

Taking the time derivative gives

$$\rho C_v \frac{\partial \theta}{\partial t} = \theta_0 \frac{\partial \eta}{\partial t} - \theta_0 f_{ij} \frac{\partial S_{ij}}{\partial t} - \theta_0 p_i \frac{\partial E_i}{\partial t} \tag{4.6.3}$$

The balance equation for entropy can be expressed as [16]

$$\frac{d}{dt} \int_V \eta \, dV = - \int_{\partial V} \Omega \cdot \mathbf{n} \, dS + \int_S \rho \sigma_s \, dV \tag{4.6.4}$$

where σ_s is the rate of internal entropy production per unit mass and Ω is the entropy flux. When (4.6.4) is valid for any part of the body, we obtain the local production of entropy [16]

$$\rho \sigma_s = \frac{\partial \eta}{\partial t} + \nabla \cdot \Omega \geq 0 \qquad \text{Clausius-Duhem inequality} \tag{4.6.5}$$

For a simple thermodynamic process, in which there are no chemical reactions and matter transfers, the entropy flux can be expressed simply by [16]

$$\Omega = \frac{q_i}{\theta_0} \tag{4.6.6}$$

where q_i is a component of the heat flux vector. In the absence of heat sources, the local balance of entropy now reads

$$\theta_0 \frac{\partial \eta}{\partial t} = - \frac{\partial q_i}{\partial x_i} \tag{4.6.7}$$

which is the equation of heat conduction in dielectrics in the absence of heat sources. Substituting (4.6.7) into (4.6.3) gives

$$\rho C_v \frac{\partial \theta}{\partial t} = - \frac{\partial q_i}{\partial x_i} - \theta_0 f_{ij} \frac{\partial S_{ij}}{\partial t} - \theta_0 p_i \frac{\partial E_i}{\partial t} \tag{4.6.8}$$

Fourier's law states that

$$q_i = \kappa_{ij} \theta_0 Q_j \tag{4.6.9}$$

where Q_j are components of the heat strain vector, $Q_j = -\frac{1}{\theta_0} \frac{\partial \theta}{\partial x_i}$ By inserting this into (4.6.8), we get the linearized heat conduction equation

$$\rho C_v \frac{\partial \theta}{\partial t} = \frac{\partial}{\partial x_i} \left(\kappa_{ij} \frac{\partial \theta}{\partial x_j} \right) - \theta_0 f_{ij} \frac{\partial^2 U_i}{\partial t \partial x_j} - \theta_0 p_i \frac{\partial E_i}{\partial t} \tag{4.6.10}$$

4.6.3 Electro-quasistatic approximation

The charge equation of electrostatics at the electro-quasistatic approximation given by

$$\nabla \cdot \mathbf{D} = \rho_e \tag{4.6.11}$$

The electric displacement for the thermopiezoelectric system is given by (4.5.13). In the quasistatic approximation, we consider polarizable (but not magnetizable) dielectrics only, with no free surface or volume charges. We can set $\rho_e = 0$, and (4.6.11) becomes (in tensor notation)

$$\frac{\partial D_i}{\partial x_i} = 0 \tag{4.6.12}$$

Substituting (4.5.13) into (4.6.12) gives the last field equation.

$$\frac{\partial}{\partial x_i}\left(e^{\theta}_{ijk} S_{jk} + \varepsilon^{S,\theta}_{ij} E_j + p^S_i \theta\right) = 0 \tag{4.6.13}$$

Since we assume $\frac{\partial D_i}{\partial x_i} = 0$, the expression within the paranthesis must be a constant. This constant is set to $-\sigma$, which is the charge specified at $x_3 = L$.

$$e^{\theta}_{ijk} S_{jk} + \varepsilon^{S,\theta}_{ij} E_j + p^S_i \theta = -\sigma \tag{4.6.14}$$

4.7 Deriving the equation set for the thermopiezoelectric solid

We assume timeharmonic behaviour and define

$$\begin{aligned} U_i &= \mathbb{R}\{\hat{U}_i e^{i\omega t}\} \\ \sigma &= \mathbb{R}\{\hat{\sigma} e^{i\omega t}\} \\ \theta &= \mathbb{R}\{\hat{\theta} e^{i\omega t}\} \\ E_i &= \mathbb{R}\{\hat{E}_i e^{i\omega t}\} \end{aligned} \tag{4.7.1}$$

where $\hat{U}_i$, $\hat{\sigma}$, $\hat{\theta}$ and $\hat{E}_i$ are complex amplitudes. From section 4.6 we have the governing field equations.

$$\rho \frac{\partial^2 U_i}{\partial t^2} = \frac{\partial}{\partial x_i}(c_{ijkl}\, S_{kl} - e_{kij}\, E_k - f_{ij}\, \theta) \tag{4.7.2a}$$

$$\rho C_v \frac{\partial \theta}{\partial t} = \frac{\partial}{\partial x_i}\left(\kappa_{ij} \frac{\partial \theta}{\partial x_j}\right) - \theta_0 f_{ij} \frac{\partial^2 U_i}{\partial t \partial x_j} - \theta_0 p_i \frac{\partial E_i}{\partial t} \tag{4.7.2b}$$

$$e_{ijk} S_{jk} + \varepsilon_{ij} E_j + p^S_i \theta = -\sigma \tag{4.7.2c}$$

4.7.1 Removing the time dependency

The timeharmonic behaviour is introduced into (4.7.2c) by applying (4.7.1), and differentiating wrt. time.

$$\mathbb{R}\left\{ e_{ijk} \frac{\partial \hat{U}_j}{\partial x_k} e^{i\omega t} + \varepsilon_{ij} \hat{E}_j e^{i\omega t} + p_i \hat{\theta} e^{i\omega t} \right\} = \mathbb{R}\left\{ -\hat{\sigma} e^{i\omega t} \right\} \tag{4.7.3}$$

$\mathbb{R}\{e^{i\omega t}\}$ is a common factor which can be factorized out to obtain a simpler expression

$$-\hat{\sigma} = e_{ijk}\frac{\partial \hat{U}_j}{\partial x_k} + \varepsilon_{ij}\hat{E}_j + p_i\hat{\theta} \tag{4.7.4}$$

We are interested in removing the dependency on the electric field from the resulting field equations, and it is then suitable to rearrange (4.7.4) wrt. $\hat{E}_3$

$$\hat{E}_j = -\frac{e_{ijk}}{\varepsilon_{ij}}\frac{\partial \hat{U}_j}{\partial x_k} - \frac{p_i}{\varepsilon_{ij}}\hat{\theta} - \frac{1}{\varepsilon_{ij}}\hat{\sigma} \tag{4.7.5}$$

Equation of motion

The same procedure is applied to the equation of motion (4.7.2a)

$$\mathbb{R}\{-\omega^2\rho\hat{U}_i e^{i\omega t}\} = \mathbb{R}\left\{c_{ijkl}\frac{\partial^2 \hat{U}_k}{\partial x_j \partial x_l}e^{i\omega t} - e_{kij}\frac{\partial \hat{E}_k}{\partial x_j}e^{i\omega t} - f_{ij}\frac{\partial \hat{\theta}}{\partial x_j}e^{i\omega t}\right\} \tag{4.7.6}$$

and the $\mathbb{R}\{e^{i\omega t}\}$ is factored out

$$-\omega^2\rho\hat{U}_i = c_{ijkl}\frac{\partial^2 \hat{U}_k}{\partial x_j \partial x_l} - e_{kij}\frac{\partial \hat{E}_k}{\partial x_j} - f_{ij}\frac{\partial \hat{\theta}}{\partial x_j} \tag{4.7.7}$$

Heat equation

The same procedure is applied to the heat equation (4.7.2b)

$$\mathbb{R}\left\{i\omega\rho C_v\hat{\theta}e^{i\omega t}\right\} = \mathbb{R}\left\{\kappa_{ij}\frac{\partial^2 \hat{\theta}}{\partial x_j^2}e^{i\omega t} - i\omega\theta_0 f_{ij}\frac{\partial \hat{U}_i}{\partial x_j}e^{i\omega t} - i\omega\theta_0 p_i\hat{E}_i e^{i\omega t}\right\} \tag{4.7.8}$$

and the $\mathbb{R}\{e^{i\omega t}\}$ is factored out

$$i\omega\rho C_v\hat{\theta} = \kappa_{ij}\frac{\partial^2 \hat{\theta}}{\partial x_j^2} - i\omega\theta_0\left(f_{ij}\frac{\partial \hat{U}_i}{\partial x_j} + p_i\hat{E}_i\right) \tag{4.7.9}$$

4.7.2 Simplify the field equations

The field equations are now timeharmonic. The matrix notation is introduced, where $ij = p$ and $kl = q$.

$$\hat{E}_j = -\frac{e_{pk}}{\varepsilon_p}\frac{\partial \hat{U}_j}{\partial x_k} - \frac{p_i}{\varepsilon_p}\hat{\theta} - \frac{1}{\varepsilon_p}\hat{\sigma} \tag{4.7.10}$$

$$-\omega^2\rho\hat{U}_i = c_{pq}\frac{\partial^2 \hat{U}_k}{\partial x_j \partial x_l} - e_{kp}\frac{\partial \hat{E}_k}{\partial x_j} - f_p\frac{\partial \hat{\theta}}{\partial x_j} \tag{4.7.11}$$

$$i\omega\rho C_v\hat{\theta}i = \kappa_p\frac{\partial^2\hat{\theta}}{\partial x_j^2} - i\omega\theta_0\left(f_p\frac{\partial \hat{U}_i}{\partial x_j} + p_i\hat{E}_i\right) \tag{4.7.12}$$

In these calculations, displacement and electric field are only allowed in the x_3-direction. The following restrictions apply

$$\begin{aligned} \frac{\partial}{\partial x_1} &= \frac{\partial}{\partial x_2} = 0 \\ U_1 &= U_2 = 0 \\ E_1 &= E_2 = 0 \end{aligned} \tag{4.7.13}$$

This results in the following equation set

$$\hat{E}_3 = -\frac{e_{33}}{\varepsilon_3}\frac{\partial \hat{U}_3}{\partial x_3} - \frac{p_3}{\varepsilon_3}\hat{\theta} - \frac{1}{\varepsilon_3}\hat{\sigma} \tag{4.7.14}$$

$$-\omega^2\rho\hat{U}_3 = c_{33}\frac{\partial^2 \hat{U}_3}{\partial x_3 \partial x_3} - e_{33}\frac{\partial \hat{E}_3}{\partial x_3} - f_3\frac{\partial \hat{\theta}}{\partial x_3} \tag{4.7.15}$$

$$i\omega\rho C_v\hat{\theta} = \kappa_3\frac{\partial^2\hat{\theta}}{\partial x_3^2} - i\omega\theta_0\left(f_3\frac{\partial \hat{U}_3}{\partial x_3} + p_3\hat{E}_3\right) \tag{4.7.16}$$

4.7.3 Removing the dependency on the electric field

The dependency on the electric field will be removed, so we will have two resulting field equations with displacement U_3 and θ as independent variables.

(4.7.14) is substitued into (4.7.15) to remove the $\hat{E}_3$ dependency. The superscripts for the material coefficients are reintroduced.

$$-\omega^2\rho\hat{U}_3 = c_{33}^{E,\theta}\frac{\partial^2 \hat{U}_3}{\partial x_3^2} - f_3^E\frac{\partial \hat{\theta}}{\partial x_3} - e_{33}^{\theta}\frac{\partial}{\partial x_3}\left(-\frac{e_{33}^{\theta}}{\varepsilon_3^S}\frac{\partial \hat{U}_3}{\partial x_3} - \frac{p_3^S}{\varepsilon_3^S}\hat{\theta} - \frac{1}{\varepsilon_3^S}\hat{\sigma}\right) \tag{4.7.17}$$

which is rearranged into

$$-\omega^2\rho\hat{U}_3 = c_{33}^{D,\theta}\frac{\partial^2 \hat{U}_3}{\partial x_3^2} - f_3^D\frac{\partial \hat{\theta}}{\partial x_3} + \left(\frac{e_{33}^{\theta}}{\varepsilon_3^S}\right)\frac{\partial \hat{\sigma}}{\partial x_3} \tag{4.7.18}$$

where $c_{33}^{D,\theta} = c_{33}^{E,\theta} + \frac{(e_{33}^{\theta})^2}{\varepsilon_3^S}$ and $f_3^D = f_3^E - \frac{e_{33}^{\theta} p_3^S}{\varepsilon_3^S}$. The last term in (4.7.18) takes account of the charge density through the structure. Since we have defined this to be a constant at a specific location ($x_3 = L$), this term is neglected in the further calculations.

For the heat equation, the same procedure is applied

$$i\omega\rho C_v^E \hat{\theta} = \kappa_3 \frac{\partial^2 \hat{\theta}}{\partial x_3^2} - i\omega\theta_0 f_3^E \frac{\partial \hat{U}_3}{\partial x_3} - i\omega\theta_0 p_3^S \left(-\frac{1}{\varepsilon_3^S}\hat{\sigma} - \frac{e_{33}^{\theta}}{\varepsilon_{33}^S}\frac{\partial \hat{U}_3}{\partial x_3} - \frac{p_3^S}{\varepsilon_3^S}\hat{\theta} \right) \tag{4.7.19}$$

and the equation is simplified to

$$i\omega\rho C_v^D \hat{\theta} = \kappa_3 \frac{\partial^2 \hat{\theta}}{\partial x_3^2} - i\omega\theta_0 f_3^D \frac{\partial \hat{U}_3}{\partial x_3} + i\omega \frac{\theta_0 p_3^S}{\varepsilon_3^S}\hat{\sigma} \tag{4.7.20}$$

where $C_V^D = C_V^E - \frac{\theta_0 (p_3^S)^2}{\rho \varepsilon_3^S}$.

The complete equation set for the structure is

$$-\omega^2 \rho \hat{U}_3 = c_{33}^{D,\theta} \frac{\partial^2 \hat{U}_3}{\partial x_3^2} - f_3^D \frac{\partial \hat{\theta}}{\partial x_3} + \left(\frac{e_{33}^{\theta}}{\varepsilon_3^S} \right) \frac{\partial \hat{\sigma}}{\partial x_3} \tag{4.7.21a}$$

$$i\omega\rho C_v^D \hat{\theta} = \kappa_3 \frac{\partial^2 \hat{\theta}}{\partial x_3^2} - i\omega\theta_0 f_3^D \frac{\partial \hat{U}_3}{\partial x_3} + i\omega \frac{\theta_0 p_3^S}{\varepsilon_3^S}\hat{\sigma} \tag{4.7.21b}$$

This equation set will consist of a homogenous and a particular solution. The homogenous solutions will be found through the eigenvalue computatios. The particular solutions are found easily by considering the equation set; For the mechanical equation, the particular solution is $\hat{U}_p = 0$, since the charge gradient is neglected. For the heat equation, the last term is a constant. By dividing the last term by the constant terms on the left side of the equation, this results in

$$\hat{\theta}_p = \frac{i\omega \frac{\theta_0 p_3^S}{\varepsilon_3^S}}{i\omega\rho C_V^D}\hat{\sigma} = \frac{\theta_0 p_3^S}{\rho C_V^D \varepsilon_3^S}\hat{\sigma} \tag{4.7.22}$$

4.8 Plane-wave solution

A plane-wave solution will be used to formulate the homogenous equation system

$$\begin{aligned} \hat{U}_3 &= \hat{U}_3 e^{-ikx_3} \\ \hat{\theta} &= \hat{\theta} e^{-ikx_3} \end{aligned} \tag{4.8.1}$$

(4.8.1) is inserted into (4.7.21) and the appropriate terms are differentiated, to obtain an equation system on the form

$$\begin{bmatrix} -\rho\omega^2 & 0 \\ 0 & i\omega\rho C_V^D \end{bmatrix} \begin{Bmatrix} \hat{U}_3 \\ \hat{\theta} \end{Bmatrix} = k^2 \begin{bmatrix} -c_{33}^{D,\theta} & 0 \\ 0 & -\kappa_3 \end{bmatrix} \begin{Bmatrix} \hat{U}_3 \\ \hat{\theta} \end{Bmatrix} + k \begin{bmatrix} 0 & if_3^D \\ -\omega\theta_0 f_3^D & 0 \end{bmatrix} \begin{Bmatrix} \hat{U}_3 \\ \hat{\theta} \end{Bmatrix} \tag{4.8.2}$$

The matrix system is on the form

$$\mathbf{Ax} = k^2\mathbf{Bx} + k\mathbf{Cx} \tag{4.8.3}$$

By choosing $\mathbf{y} = k\mathbf{Bx}$ we can reduce the problem to a generalized eigenvalue problem (4.8.5)

$$\begin{aligned} \mathbf{Y} &= k\mathbf{Bx} \\ \mathbf{Ax} &= k\mathbf{Y} + k\mathbf{Cx} \end{aligned} \tag{4.8.4}$$

A generalized eigenvalue problem is on the form

$$\mathbf{Ax} = \lambda\mathbf{Bx} \tag{4.8.5}$$

Setting (4.8.4) up as a matrix system

$$\begin{bmatrix} \mathbf{A} & \mathbf{0} \\ \mathbf{0} & \mathbf{I} \end{bmatrix} \begin{Bmatrix} x \\ y \end{Bmatrix} = k \begin{bmatrix} \mathbf{C} & \mathbf{I} \\ \mathbf{B} & \mathbf{0} \end{bmatrix} \begin{Bmatrix} x \\ y \end{Bmatrix} \qquad \text{where } x = \begin{Bmatrix} \hat{U}_3 \\ \hat{\theta} \end{Bmatrix} \tag{4.8.6}$$

This is implemented in Matlab. Using the `eig()`-function, we get a 4×4-matrix with eigenvectors on the columns, and a 4×4 diagonal matrix with the eigenvalues, k_n. We have a general solution on the form

$$\begin{Bmatrix} \hat{U} \\ \hat{\theta} \end{Bmatrix} = A_1 \begin{bmatrix} \hat{U}_{g1} \\ \hat{\theta}_{g1} \end{bmatrix} e^{-ik_1 x} + A_2 \begin{bmatrix} \hat{U}_{g2} \\ \hat{\theta}_{g2} \end{bmatrix} e^{-ik_2 x} + A_3 \begin{bmatrix} \hat{U}_{g3} \\ \hat{\theta}_{g3} \end{bmatrix} e^{-ik_3 x} + A_4 \begin{bmatrix} \hat{U}_{g4} \\ \hat{\theta}_{g4} \end{bmatrix} e^{-ik_4 x} \tag{4.8.7}$$

(4.8.7) can be set up as a matrix equation

$$\begin{Bmatrix} \hat{U} \\ \hat{\theta} \end{Bmatrix} = \begin{bmatrix} \hat{U}_{g1} & \hat{U}_{g2} & \hat{U}_{g3} & \hat{U}_{g4} \\ \hat{\theta}_{g1} & \hat{\theta}_{g2} & \hat{\theta}_{g4} & \hat{\theta}_{g4} \end{bmatrix} \begin{bmatrix} e^{-ik_1 x} & & & \\ & e^{-ik_2 x} & & \\ & & e^{-ik_3 x} & \\ & & & e^{-ik_4 x} \end{bmatrix} \begin{Bmatrix} A_1 \\ A_2 \\ A_3 \\ A_4 \end{Bmatrix} \tag{4.8.8}$$

Only the top two rows in the eigenvector matrix is used, see (4.8.6)

4.8.1 Dimensionless form

To avoid numerically unstable eigenvalues and eigenvectors, it is preferred to formulate the problem in dimensionless form. This problem has a wide range of dimensions, from sub-nanometer displacements to several Gigahertz, which causes an unbalanced equation set. We have the equation set from (4.8.2)

$$-\rho\omega^2\hat{U}_3 = k^2\left(-c_{33}^{D,\theta}\right)\hat{U}_3 + k(if_3^D)\hat{\theta} \tag{4.8.9a}$$

$$i\omega\rho C_V^D\hat{\theta} = k^2(-\kappa_3)\hat{\theta} + k(-i\omega\theta_0 f_3^D)\hat{U}_3 \tag{4.8.9b}$$

Dividing (4.8.9a) by $\left(-c_{33}^{D,\theta}\right)$ gives

$$k_m^2\hat{U}_3 = k^2\hat{U}_3 + k\left(-i\frac{f_3^D}{c_{33}^{D,\theta}}\right)\hat{\theta} \tag{4.8.10}$$

where $k_m^2 = \frac{\rho\omega^2}{c_{33}^{D,\theta}}$. Dividing (4.8.9b) by $(-\kappa_3)$ gives

$$-ik_t^2\hat{\theta} = k^2\hat{\theta} + k\left(\frac{\omega\theta_0 f_3^D}{\kappa_3}\right)\hat{U}_3 \tag{4.8.11}$$

where $k_t^2 = \frac{\omega\rho C_V^D}{\kappa_3}$. Now we have a matrix system of the form

$$\begin{bmatrix} k_m^2 & \\ & -ik_t^2 \end{bmatrix}\begin{Bmatrix}\hat{U}_3\\ \hat{\theta}\end{Bmatrix} = k^2\begin{Bmatrix}\hat{U}_3\\ \hat{\theta}\end{Bmatrix} + k\begin{bmatrix} & -i\frac{f_3^D}{c_{33}^{D,\theta}}\\ \frac{\omega\theta_0 f_3^D}{\kappa_3} & \end{bmatrix}\begin{Bmatrix}\hat{U}_3\\ \hat{\theta}\end{Bmatrix} \tag{4.8.12}$$

Choosing the dimensionless variables, γ and τ, to replace $\hat{U}_3$ and $\hat{\theta}$

$$\begin{aligned}\gamma &= \lambda\hat{U}_3\\ \tau &= \mu\hat{\theta}\end{aligned} \tag{4.8.13}$$

where λ and μ are variables connecting the normal and dimensionless form. Substuting (4.8.13) into (4.8.10) and (4.8.11) gives

$$\begin{aligned}k_m^2\gamma &= k^2\gamma - ikf_3^D\left(\frac{\lambda}{c_{33}^{D,\theta}\mu}\right)\tau\\ -ik_t^2\tau &= k^2\tau + kf_3^D\left(\frac{\omega\theta_0\mu}{\kappa_3\lambda}\right)\gamma\end{aligned} \tag{4.8.14}$$

Setting the expressions enclosed in parantheses equal will give a relationship between the non-dimensionless variables.

$$\frac{\lambda}{c_{33}^{D,\theta}\mu} = \frac{\omega\theta_0\mu}{\kappa_3\lambda} \Longrightarrow \frac{\lambda}{\mu} = \sqrt{\frac{\omega\theta_0 c_{33}^{D,\theta}}{\kappa_3}} \tag{4.8.15}$$

A sensible choice for μ would be $\mu = \frac{1}{\theta_0}$, since this would give no dimension on the temperature. Substituting into (4.8.15) gives

$$\lambda = \sqrt{\frac{\omega c_{33}^{D,\theta}}{\kappa_3\theta_0}} \tag{4.8.16}$$

Inserting for μ and λ into (4.8.14) gives

$$\begin{aligned}k_m^2\gamma &= k^2\gamma - ikf_3^D\zeta\tau\\ -ik_t^2\tau &= k^2\tau + kf_3^D\zeta\gamma\end{aligned} \tag{4.8.17}$$

where $\zeta = \sqrt{\frac{\omega\theta_0}{\kappa_3 c_{33}^{D,\theta}}}$. Now we have a dimensionless equation system, and is shown here in matrix form.

$$\begin{bmatrix} k_m^2 & \\ & -ik_t^2 \end{bmatrix} \begin{Bmatrix} \gamma \\ \tau \end{Bmatrix} = k^2 \begin{Bmatrix} \gamma \\ \tau \end{Bmatrix} + k \begin{bmatrix} & -if_3^D\zeta \\ f_3^D\zeta & \end{bmatrix} \begin{Bmatrix} \gamma \\ \tau \end{Bmatrix} \tag{4.8.18}$$

The dimensionless form replaces the equation in (4.8.2), but it is important to remember that the resulting general solution will not be U_3 and θ, but γ and τ. This means that the solution with the dimensionless variables needs to be scaled back to the original variables using

$$\begin{aligned} \gamma &= \lambda \hat{U}_3 \\ \tau &= \mu \hat{\theta} \end{aligned} \tag{4.8.19}$$

4.9 Boundary conditions

By including the thermal effects, we get a coupled system which needs to be treated differently than the pure piezoelectric problem. The general solution is now a matrix equation with block matrices instead of scalars (*See* (4.9.1)), so both the temperature/displacement and heat flux/stress are being accounted for in each of the boundary conditions.

Displacement and temperature across internal boundaries

As in the previous models, the continuity in displacement is required. The temperature also has the same requirement, to be continuous throughout the structure.

$$\begin{Bmatrix} U_3^L|_{x_3=0^-} = U_3^M|_{x_3=0^+} \\ \theta_3^L|_{x_3=0^-} = \theta_3^M|_{x_3=0^+} \end{Bmatrix} \qquad \begin{Bmatrix} U_3^M|_{x_3=L^-} = U_3^R|_{x_3=L^+} \\ \theta_3^M|_{x_3=L^-} = \theta_3^R|_{x_3=L^+} \end{Bmatrix}$$

Stress/heat flux continuity across internal boundaries The stress and the heat flux must be continuous across the internal boundaries

$$\begin{Bmatrix} T_3^L|_{x_3=0^-} = T_3^M|_{x_3=0^+} \\ q_3^L|_{x_3=0^-} = q_3^M|_{x_3=0^+} \end{Bmatrix} \qquad \begin{Bmatrix} T_3^M|_{x_3=L^-} = T_3^R|_{x_3=L^+} \\ q_3^M|_{x_3=L^-} = q_3^R|_{x_3=L^+} \end{Bmatrix}$$

Free ends There must be no stress at the ends in order for the structure to be freely vibrating. The heat flux must also be zero, so we don't have any heat dissipating out of the structure.

$$\begin{Bmatrix} T_3^L|_{x_3=-t} = 0 \\ q_3^L|_{x_3=-t} = 0 \end{Bmatrix} \qquad \begin{Bmatrix} T_3^R|_{x_3=L+t} = 0 \\ q_3^R|_{x_3=L+t} = 0 \end{Bmatrix}$$

4.9.1 Applying the boundary conditions

These boundary conditions are applied to the total solution

$$\begin{Bmatrix} \hat{U} \\ \hat{\theta} \end{Bmatrix} = \begin{bmatrix} \hat{U}_{g1} & \hat{U}_{g2} & \hat{U}_{g3} & \hat{U}_{g4} \\ \hat{\theta}_{g1} & \hat{\theta}_{g2} & \hat{\theta}_{g4} & \hat{\theta}_{g4} \end{bmatrix} \begin{bmatrix} e^{-ik_1x_3} & & & \\ & e^{-ik_2x_3} & & \\ & & e^{-ik_3x_3} & \\ & & & e^{-ik_4x_3} \end{bmatrix} \begin{Bmatrix} A_1 \\ A_2 \\ A_3 \\ A_4 \end{Bmatrix} + \begin{Bmatrix} \hat{U}_p \\ \hat{\theta}_p \end{Bmatrix} \quad (4.9.1)$$

To ease the notation, (4.9.1), is written in the following way

$$\mathbf{V}_n\mathbf{Z}_n(x_3)\mathbf{A} + \mathbf{P}_n \quad (4.9.2)$$

where n is the layer and x_3 is the position along the x_3 axis.

Displacement and temperature across internal boundaries

(4.9.2) is inserted into the boundary conditions, and we get the following block matrix equation

$$\mathbf{V}_L\mathbf{Z}_L(0) + \mathbf{P}_L = \mathbf{V}_M\mathbf{Z}_M(0) + \mathbf{P}_M$$

Reordering the equation to have the particular solution on the right hand side.

$$\mathbf{V}_L\mathbf{Z}_L(0) - \mathbf{V}_M\mathbf{Z}_M(0) = \mathbf{P}_M - \mathbf{P}_L \quad (4.9.3)$$

Similarly for the same boundary condition at $x_3 = L$

$$\mathbf{V}_M\mathbf{Z}_M(L) - \mathbf{V}_R\mathbf{Z}_R(L) = \mathbf{P}_R - \mathbf{P}_M \quad (4.9.4)$$

Stress/heat flux continuity across internal borders

Stress and heat flux are defined in the constitutive equations and utilizing Fourier's law respectively. Stress including thermal effects is given by (superscripts neglected)

$$T_{ij} = c_{ijkl}S_{kl} - e_{kij}E_k - f_{ij}\theta \quad (4.9.5)$$

From Fourier's law, the heat flux is defined as

$$q_i = -\kappa_{ij}\frac{\partial\theta}{\partial x_k} \quad (4.9.6)$$

where q_i is the heat flux and κ_{ij} are components of the heat conductivity tensor. We only consider displacement in the x_3-direction, which reduces (4.9.5) and (4.9.6) into (using matrix notation)

$$T_3 = c_{33}S_{kl} - e_{kij}E_k - f_{ij}\theta \quad (4.9.7a)$$

$$q_3 = -\kappa_3\frac{\partial\theta}{\partial x_3} \quad (4.9.7b)$$

We want to eliminate the electric field, so the stress becomes a function of U_3 and θ. From 4.7.5, removing the hats and superscripts, we have

$$E_3 = -\frac{e_{33}}{\varepsilon_3}\frac{\partial U_3}{\partial x_3} - \frac{p_3}{\varepsilon_3}\theta - \frac{1}{\varepsilon_3}\sigma \tag{4.9.8}$$

Substituting (4.9.8) into (4.7.7a) reduces the stress equation to having two independent variables in addition to the σ variable which will be the particular solution of the problem.

$$\begin{aligned} T_3 &= c_{33}U_{3,3} - f_3\theta - e_{33}\left(-\frac{e_{33}}{\varepsilon_3}\frac{\partial U_3}{\partial x_3} - \frac{p_3}{\varepsilon_3}\theta - \frac{1}{\varepsilon_3}\sigma\right) \\ &= c_{33}^D\frac{\partial U_3}{\partial x_3} - f_3^D\theta + \frac{e_{33}}{\varepsilon_3^S}\sigma \end{aligned} \tag{4.9.9}$$

In order to realize (4.9.9) and (4.9.6), we must introduce two material property matrices and a differentiation matrix. The material property matrices are

$$\mathbf{M}_d = \begin{bmatrix} c_{33}^D & \\ & -\kappa_3 \end{bmatrix} \qquad \mathbf{M}_{od} = \begin{bmatrix} & -f_{ij} \\ & \end{bmatrix} \tag{4.9.10}$$

and the differentiation matrix is

$$\mathbf{D} = \begin{bmatrix} -ik_1 & & & \\ & -ik_2 & & \\ & & -ik_3 & \\ & & & -ik_4 \end{bmatrix} \tag{4.9.11}$$

The boundary condition for stress/heat flux at $x_3 = 0$ then becomes

$$\left(\mathbf{M}_d^L\mathbf{V}^L\mathbf{D}^L + \mathbf{M}_{od}^L\mathbf{V}^L\right)\mathbf{Z}^L(0) = \left(\mathbf{M}_d^M\mathbf{V}^M\mathbf{D}^M + \mathbf{M}_{od}^M\mathbf{V}^M\right)\mathbf{Z}^M(0) \tag{4.9.12}$$

and for $x_3 = L$

$$\left(\mathbf{M}_d^M\mathbf{V}^M\mathbf{D}^M + \mathbf{M}_{od}^M\mathbf{V}^M\right)\mathbf{Z}^M(L) = \left(\mathbf{M}_d^R\mathbf{V}^R\mathbf{D}^R + \mathbf{M}_{od}^R\mathbf{V}^R\right)\mathbf{Z}^R(L) \tag{4.9.13}$$

No stress/heat flux at the ends

The same boundary condition for the piezoelectric model is used for the stress, but in addition we have the condition for no heat flux at the end. This ensures that no heat flux radiates out of the structure, but is confined within the structure.

$$\left\{\begin{matrix} \frac{\partial T_3^L}{\partial x_3}|_{x_3=-t} = 0 \\ \frac{\partial q_3^L}{\partial x_3}|_{x_3=-t} = 0 \end{matrix}\right\} \qquad \left\{\begin{matrix} \frac{\partial T_3^R}{\partial x_3}|_{x_3=L+t} = 0 \\ \frac{\partial q_3^R}{\partial x_3}|_{x_3=L+t} = 0 \end{matrix}\right\}$$

By applying the matrix form of the general solution and the material and differentiation matrices, we get the following boundary conditions for $x_3 = -t$

$$\left(\mathbf{M}_d^L \mathbf{V}^L \mathbf{D}^L + \mathbf{M}_{od}^L \mathbf{V}^L\right) \mathbf{Z}^L(-t) = 0 \tag{4.9.14}$$

and for $x_3 = L + t$

$$\left(\mathbf{M}_d^R \mathbf{V}^R \mathbf{D}^R + \mathbf{M}_{od}^R \mathbf{V}^R\right) \mathbf{Z}^R(L+t) = 0 \tag{4.9.15}$$

All of the boundary condition, except for the particular solutions, are collected in a matrix

$$\mathbf{K} = \begin{bmatrix} \mathbf{V}^L \mathbf{Z}^L(0) & -\mathbf{V}^M \mathbf{Z}^M(0) & \mathbf{0} \\ \mathbf{0} & \mathbf{V}^M \mathbf{Z}^M(L) & -\mathbf{V}^R \mathbf{Z}^R(L) \\ \left(\mathbf{M}_d^L \mathbf{V}^L \mathbf{D}^L + \mathbf{M}_{od}^L \mathbf{V}^L\right) \mathbf{Z}^L(0) & -\left(\mathbf{M}_d^M \mathbf{V}^M \mathbf{D}^M + \mathbf{M}_{od}^M \mathbf{V}^M\right) \mathbf{Z}^M(0) & \mathbf{0} \\ \mathbf{0} & \left(\mathbf{M}_d^M \mathbf{V}^M \mathbf{D}^M + \mathbf{M}_{od}^M \mathbf{V}^M\right) \mathbf{Z}^M(L) & -\left(\mathbf{M}_d^R \mathbf{V}^R \mathbf{D}^R + \mathbf{M}_{od}^R \mathbf{V}^R\right) \mathbf{Z}^R(L) \\ \left(\mathbf{M}_d^L \mathbf{V}^L \mathbf{D}^L + \mathbf{M}_{od}^L \mathbf{V}^L\right) \mathbf{Z}^L(-t) & \mathbf{0} & \mathbf{0} \\ \mathbf{0} & \mathbf{0} & \left(\mathbf{M}_d^R \mathbf{V}^R \mathbf{D}^R + \mathbf{M}_{od}^R \mathbf{V}^R\right) \mathbf{Z}^R(L+t) \end{bmatrix}$$

which is a $12x12$ matrix. The particular solutions are gathered in a matrix

$$\mathbf{P}_{(6\times 1)} = \begin{bmatrix} -P^L + P^M \\ -P^M + P^R \\ -P^L + P^M \\ -P^M + P^R \\ -P^L \\ -P^R \end{bmatrix} \tag{4.9.16}$$

4.9.2 Electrical boundary conditions

The voltage is given by

$$V = -\frac{\partial \phi}{\partial x_3} \tag{4.9.17}$$

Inserting this into (4.5.13) and integrating through the piezoelectric layer from $x_3 = 0$ to $x_3 = L$, we get

$$-\varepsilon_3^S \underbrace{\left(\phi(L) - \phi(0)\right)}_{V} + e_{33}\left(\hat{U}_3(L) - \hat{U}_3(0)\right) + p_3 L \int_0^L \hat{\theta} dx_3 = L\hat{\sigma} \tag{4.9.18}$$

Rearranging and we get an expression for the voltage

$$V = \frac{e_{33}}{\varepsilon_3^S}\left(\hat{U}_3(L) - \hat{U}_3(0)\right) + \frac{\pi_3 L}{\varepsilon_3^S}\int_0^L \hat{\theta} dx_3 + \frac{L}{\varepsilon_3^S}\hat{\sigma} \tag{4.9.19}$$

$\hat{U}_3$ and $\hat{\theta}$ can be represented as series

$$\hat{U}_3(x_3) = \sum_{j=1}^{4} A_{mj} \hat{U}_{mj} e^{-ik_j x_3} \qquad \hat{\theta}(x_3) = \sum_{j=1}^{4} A_{mj} \hat{\theta}_{mj} e^{-ik_j x_3} \tag{4.9.20}$$

and by inserting this into (4.9.19) we get

$$V = \sum_{j=1}^{4} \left\{ \frac{e_{33}}{\varepsilon_3^S} U_{mj} \left(e^{-ik_j L} - 1 \right) + i \frac{\pi_3 L}{\varepsilon_3^S} \frac{\hat{\theta}_{mj}}{k_j} \left(e^{-ik_j L} - 1 \right) \right\} A_{mj} \tag{4.9.21}$$

where the term enclosed within the curly brackets is called the T_{mj}-vector which has the form

$$T_{(1\times 12)} = \begin{bmatrix} \mathbf{0} & T_{m1} & T_{m2} & T_{m3} & T_{m4} & \mathbf{0} \end{bmatrix} \tag{4.9.22}$$

where $\mathbf{0}$ is a (1×4) zero-matrix.

4.10 Implementing the calculations in Matlab

All the material properties are collected in a `materialTable`-matrix where each of the columns represent the materials. It is structured in the following way

$$\begin{bmatrix} \rho \\ C_V \\ p \\ \varepsilon_3^S \\ c_{33}^E \\ \kappa_{33} \\ K \\ \theta_0 \\ \alpha \\ \nu \end{bmatrix} \tag{4.10.1}$$

Due to large differences between the rows in the boundary conditions matrix, a linear scaling of the rows are being done by a scaling vector to balance the matrix. The same scaling is also applied to the **P**-matrix.

A vector which spans the frequency range of choice, is used for iterating through the procedure. The frequencies are used as an argument in a `for`-loop which handles all the eigenvalue calculations for the system.

All the calculations are solved for each layer, which are stored as structures instead of ordinary variables. This gives the possibility to store the solutions as `eigenValues.n`, where `n` is the layer name.

The impedance is calculated in the same way as for the non-thermal model, which is shown in *Section 3.6.2*.

CHAPTER 5

Results

5.1 Quality factor as a function of layer thickness

The quality factor (Q-factor) is a dimensionless, real, positive number which is used for quantifying the performance of dynamical systems. It is defined as

$$Q = \frac{\omega_s}{\omega^+ - \omega^-} \tag{5.1.1}$$

where ω^+ and ω^- are the $-3\ dB$ frequencies above and below ω_s, which defines the bandwidth. The Q-factor quantifies the energy efficiency of the system, and thus can be used to estimate the losses. In a high frequency resonator applications, a high as possible Q-factor is preferred.

In the calculations, the amplitude of the admittance is used for calculating the Q-factor. The Y_{max} frequency is used as the center frequency, and the $-3\ dB$ frequencies are used for calculating the bandwidth. To Y_{max} is normalized to the maximum value, making it easy do identify the maximum frequency ($Y = 1$), and the $3\ dB$ frequencies ($0.45 \cdot Y < Y < 0.55 \cdot Y$). The range in selecting the $-3\ dB$ frequenices are used to reduce computing time. Since the Q-factor is quite high, the frequency change is neglectible between $0.45 \cdot Y < Y < 0.55 \cdot Y$.

The Matlab algorithm for choosing the Q-factor is

```
normYabs=abs(Y)./max(abs(Y));
fs_3db=f(normYabs>0.45 & normYabs<0.55);
fs_res=f(normYabs==1);
Qs=fs_res/(max(fs_3db)-min(fs_3db))
```

5.2 Coupling factor as a function of metal layer thickness

For a Mason model of a free piezoelectric element vibrating in the thickness mode, the total impedance is given by[12]

$$Z_T = \frac{1}{i\omega C_0}\left(1 - k_t^2 \frac{\tan\left(\frac{k_m l}{2}\right)}{\frac{k_m l}{2}}\right) = iX_T \qquad R_T = 0 \tag{5.2.1}$$

where k_m is the wavenumber in the material, and k_t is the electromechanical coupling constant. The first resonance frequency for the system occurs when $Z_T = i0$ and can only be achieved when

$$\tan x_s = \frac{x_s}{k_t^2} \qquad \text{where } x_s = \frac{k_m l}{2} \tag{5.2.2}$$

The wavenumber is given by $k_m = \frac{2\pi f_1 l}{2c_m}$, where c_m is the speed of sound in the material. For the antiresonance, the condition is $Z_T = i\infty$ and requires $\tan x_p = \infty$, such that

$$x_p = \frac{2\pi f_2 l}{2c_m} = \frac{\pi}{2} \tag{5.2.3}$$

Rearranging (5.2.3) we get $f_2 = \frac{c_m}{2l}$, which is the halfwave resonance of the piezoelectric element. Using 5.2.2, inserting for x_s and solving for k_t^2 we get

$$k_t^2 = \frac{\frac{\pi f_1 l}{c_m}}{\tan\left(\frac{\pi f_1 l}{c_m}\right)} \tag{5.2.4}$$

From (5.2.3) we have $c_m = 2l f_2$, which is inserted into (5.2.4), to get

$$k_t^2 = \frac{\frac{\pi}{2}\frac{f_1}{f_2}}{\tan\left(\frac{\pi}{2}\frac{f_1}{f_2}\right)} \tag{5.2.5}$$

Using the relation

$$\frac{1}{\tan x} = \tan\left(\frac{\pi}{2} - x\right) \tag{5.2.6}$$

we get

$$k_t^2 = \frac{\pi}{2}\frac{f_1}{f_2}\tan\left(\frac{\pi}{2}\frac{f_2 - f_1}{f_2}\right) \tag{5.2.7}$$

k_{eff}^2 is extracted from the calculations and plotted as a function of metal layer thickness. 5 GHz and 10 GHz is chosen as the key frequencies to investigate, and the thickness of the piezoelectric layer is changed accordingly to each metal layer thickness, to achieve each of the frequencies. This gives us an indication of the influence of the metal layer on the energy efficiency of the FBAR structure. The thickness with the highest k_{eff}^2 then has an indicative, optimal thickness ratio between the metal electrodes and the piezoelectric layer for the given frequency.

5.3 Performance for different contact materials

With a non-thermal and a thermal model for the FBAR, the comparison of the contact materials can be done. The simulation has included the whole range of possible thicknesses for both contact and piezoelectric layer, but the most sensible results will be in the midrange around $100-150$ nm, which seems to be a more realistic thickness to use in FBAR's. The results will be compared to other references as far as it is possible, but most of the comparison will be between the results obtained in this simulation.

5.3.1 Aluminium

Aluminium is the most abundant metal in the Earth's crust, but due to its high reactivity with other minerals it is rarely found as a free metal. It has very low density and very high resistance to corrosion. It has a low bulk modulus, which means that it is a quite ductile material, and the temperature coefficient of expansion is big. It has excellent thermal properties with a high thermal conductivity and heat capacity. The device dimensions for the 5 GHz device is shown in *Table 5.1*

Figure 5.1 shows quite high coupling over a relatively large range of contact thicknesses. With the thermal effects, the coupling has a maximum at approximately 7%. The difference between the thermal and non-thermal model is apparent, and is more pronounced at the thinner contact thicknesses, where the piezoelectric layer is quite thick compared to the contacts. At the maximum contact thickness around ~ 240 nm, the contact thickness is twice as thick as the piezoelectric layer, and the coupling constant is quite similar in both models. This can be due to the mass loading of the contacts compared to the very thin piezoelectric layer.

Table 5.1: Device dimensions for *Al*-contacts

t_c 5 GHz	t_c 5 GHz	t_c 10 GHz	t_p 10 GHz
10	1109	1	561
20	1091	3	558
30	1072	5	554
50	1035	10	545
70	995	20	527
100	927	40	487
120	874	50	463
150	776	60	437
200	518	80	367
220	363	100	259
240	170	120	84

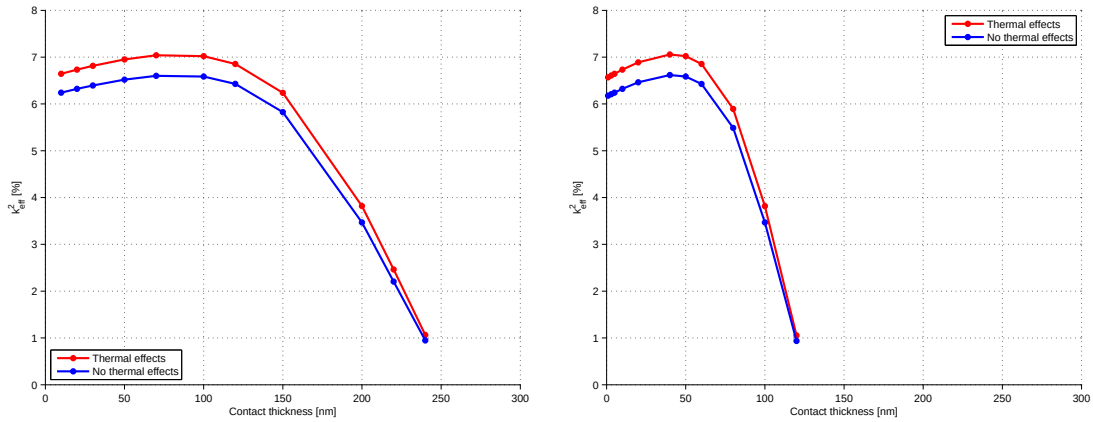

Figure 5.1: k^2_{eff} wrt. contact thickness for Aluminium at 5 GHz and 10 GHz

The Q-factor is shown in *Figure 5.2*, and the maximum is $Q \approx 28000$. For contact thicknesses larger than 150 nm, the Q-value is approximately 1000. This is a more realistic thickness in a real device, and hence Aluminium is not as well suited as a contact material. Yokoyama et al. [14] states that due to the low acoustic impedance, $Z_a = \sqrt{c \times \rho}$, Aluminium has a disadvantage with use in high frequency filters. This seems to fit well to the results from the Matlab model. *Figure 5.3* shows frequency difference between the non-thermal and thermal model. The antiresonance/resonance of the thermal model is held approximately constant at 5 GHz, and the gap up to the non-thermal model is shown in the plot. The biggest effect is seen at a contact thickness of $t_{contact} = 150$ nm, which is where the biggest gap between the two models in terms of both resonance and antiresonance frequency.

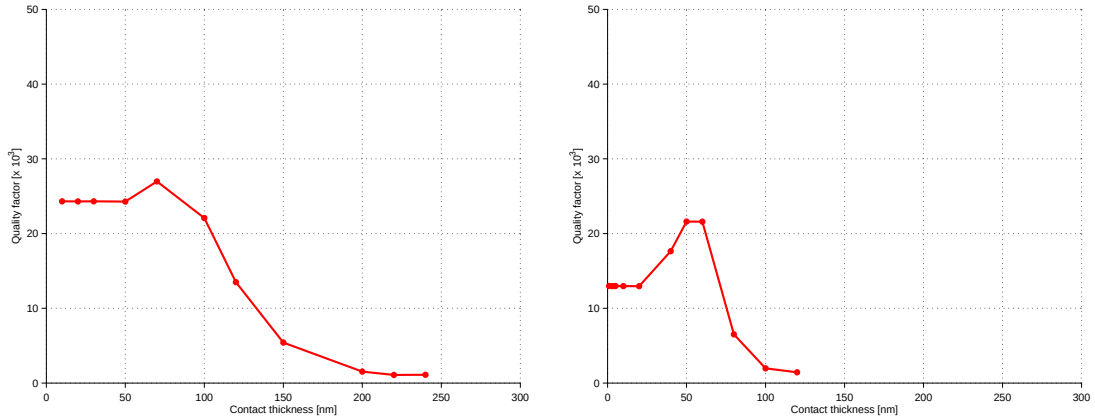

Figure 5.2: Quality factor for Aluminium at 5 GHz

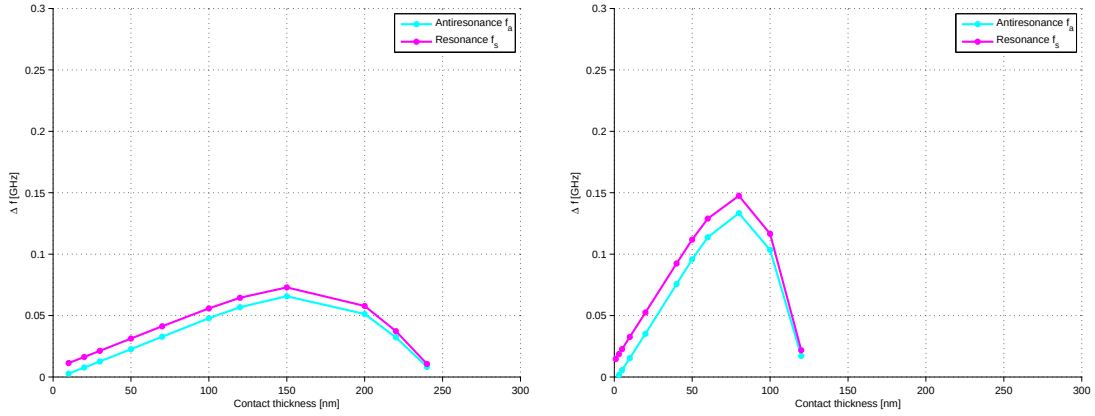

Figure 5.3: Difference between the resonant frequencies for thermal and non-thermal effects for Aluminium at 5 GHz

For the resonance frequency the frequency difference is as big as $\sim 70\ MHz$ which is a considerable amount. The cause of this difference has not been figured out, but can be due to the thermal effects introducing a lowering of the stiffness of the structure. This effect seems to increase at 10 GHz, but that can also be an effect of the relative difference of the frequencies.

5.3.2 Ruthenium

Ruthenium has shown to be a promising material for FBAR structures. It is a very tough material, used in applications where exceptional toughness is required. It is quite similar to Molybdenum in properties, but has a higher stiffness.

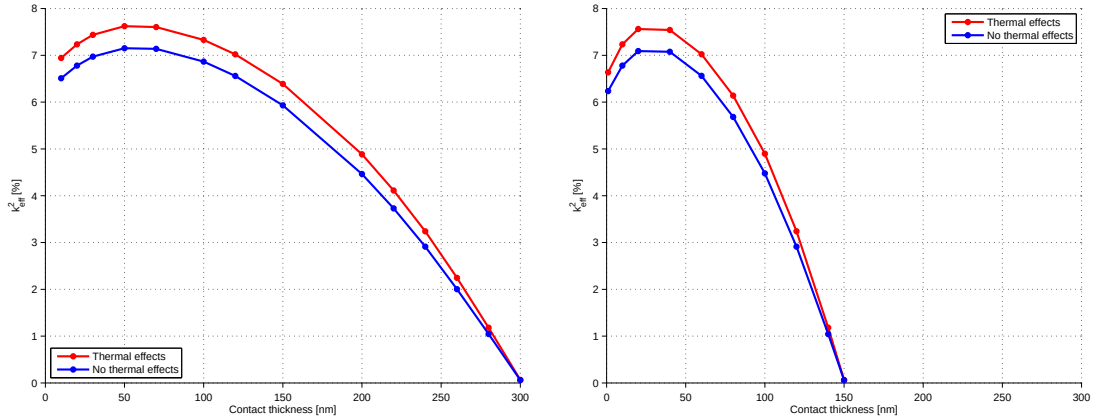

Figure 5.4: k^2_{eff} wrt. contact thickness for Ruthenium at 5 GHz and 10 GHz

Above 100 *nm*, the Q-factor is quite stable around ~ 7000. Ruthenium has found to be very suitable as an electrode material [14], which seems to fit well to our model.

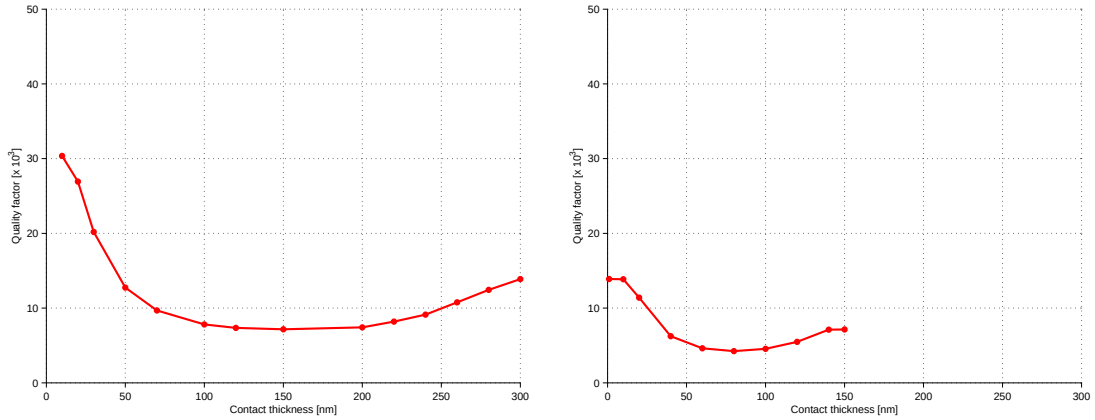

Figure 5.5: Quality factor for Ruthenium at 5 GHz and 10 GHz

Figure 5.6

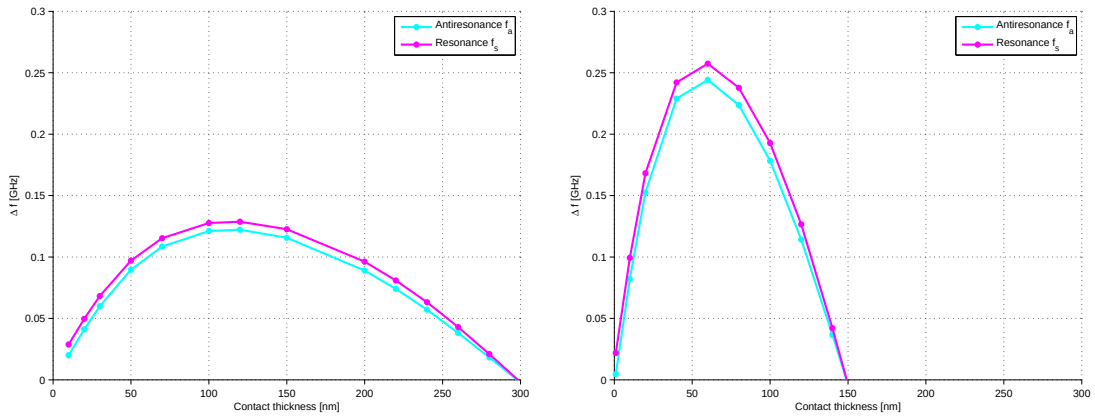

Figure 5.6: Difference between the resonant frequencies for thermal and non-thermal effects for Ruthenium at 5 GHz and 10 GHz

5.3.3 Molybdenum

Molybdenum has been widely used as an electrode material due to its low resistivity and high acoustic impedance[10]. It has a very high melting temperature and has generally high heat resistance, which makes it ideal for high temperature applications. It is widely used in manufacturing of aircraft parts, electronic components, filaments etc.

Compared to the other materials used in this thesis, it has a medium density at $\rho_0 = 10280\, kg\, m^{-3}$ and high bulk modulus $K = 230\, GPa$. The heat conductivity is quite high at $\kappa = 139\, Wm^{-1}K^{-1}$, and the temperature coefficient of expansion is quite low at $4.8 \times 10^{-6}K^{-1}$. It has the second highest heat capacity of the contact materials investigated.

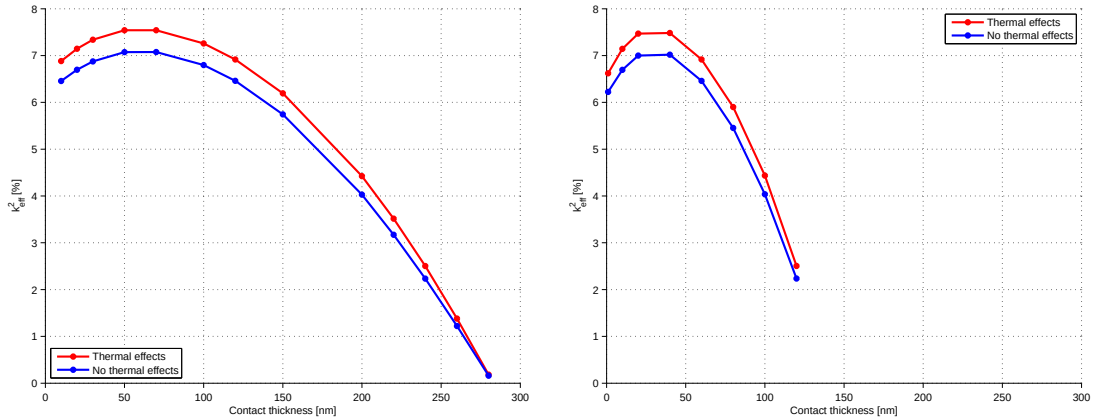

Figure 5.7: k^2_{eff} wrt. contact thickness for Molybdenum at 5 GHz and 10 GHz

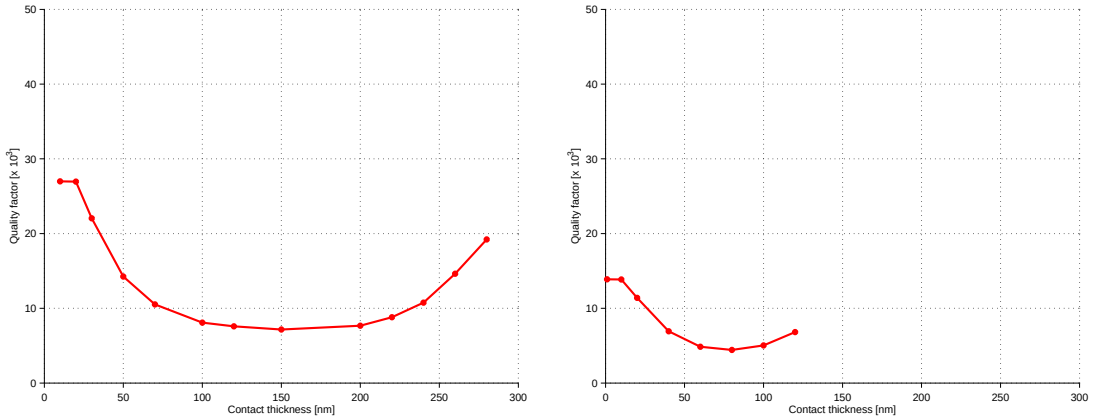

Figure 5.8: Quality factor for Molybdenum at 5 GHz and 10 GHz

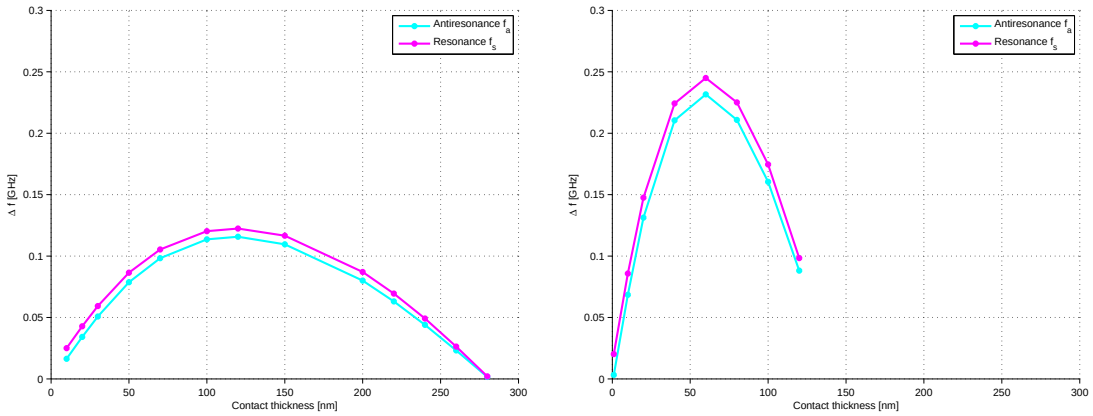

Figure 5.9: Difference between the resonant frequencies for thermal and non-thermal effects for Molybdenum at 5 GHz and 10 GHz

5.3.4 Platinum

Platinum is the most dense material with a density of 21090 $kg\ m^{-3}$, and the lowest speed of sound of 2680 $m\ s^{-1}$.

Because of this high weight density, Platinum has disadvantages for use in high frequency FBAR filters[14]. From 5.11 we can see at the mid-range contact thicknesses, that the Q-value is quite lower than most of the other materials.

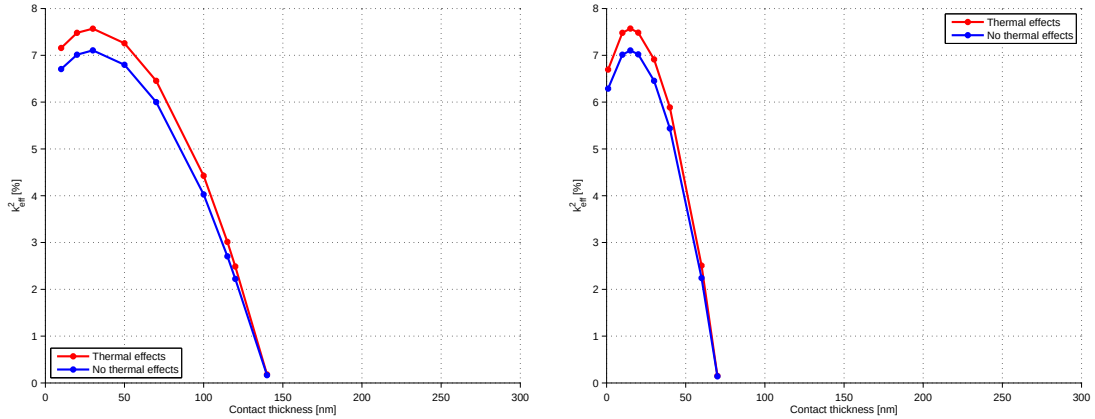

Figure 5.10: k^2_{eff} wrt. contact thickness for Platinum at 5 GHz and 10 GHz

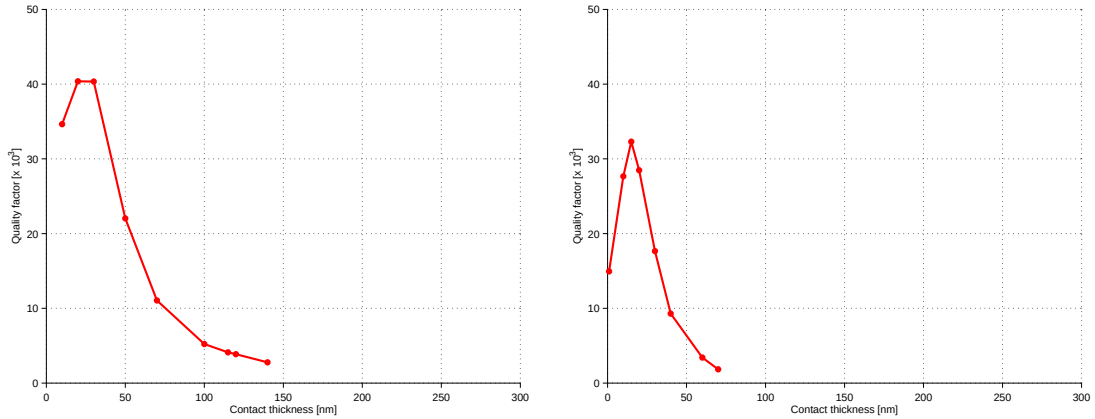

Figure 5.11: Quality factor for Platinum at 5 GHz and 10 GHz

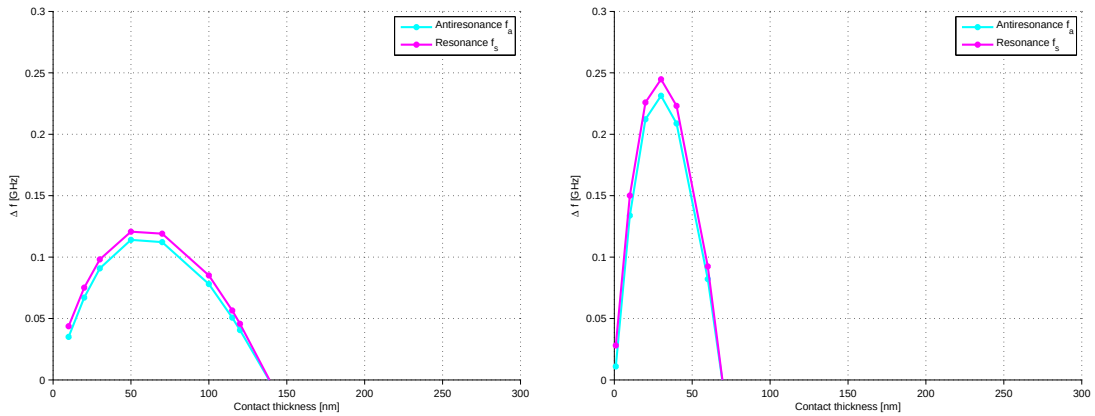

Figure 5.12: Difference between the resonant frequencies for thermal and non-thermal effects for Platinum at 5 GHz and 10 GHz

5.4 Figure of merit

There are many ways to classify the performance of mechanical devices. For FBAR's a common way to measure it is using the k_t^2Q-product as a figure of merit. The k_t^2Q-product is shown for the different materials in *Figure 5.13*

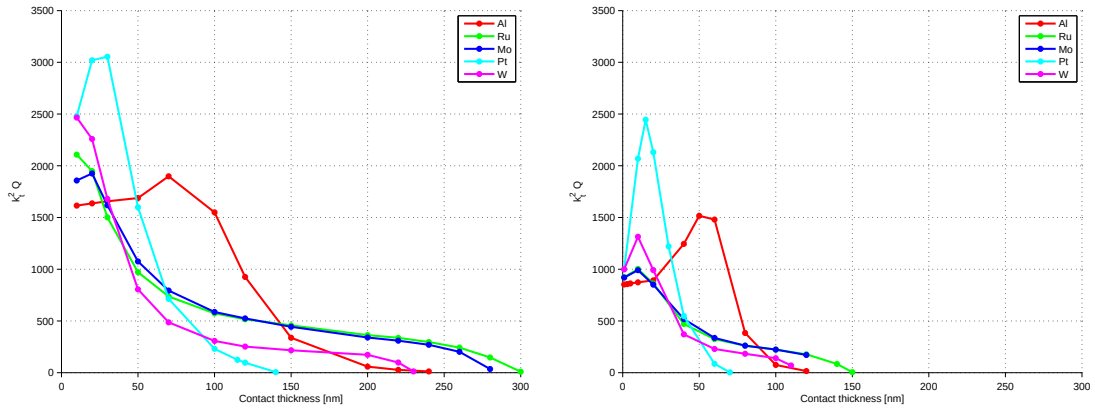

Figure 5.13: k_t^2Q-product for the different contact materials at 5 GHz and 10 GHz

5.5 Correction of results

Unfortunately, there was a small error in the Matlab model at a late time, which caused the results to be wrong. The time to reproduce all the results from scratch is not feasible, but a small example with the correct code is shown here.

Figure 5.14 shows that the coupling as close to identical for both the thermal and the non-thermal model, and differ slightly at the largest contact thicknesses.

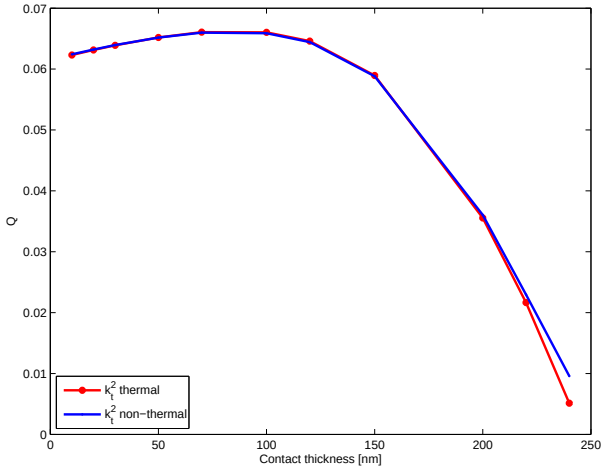

Figure 5.14: Effective coupling constant for thermal and non-thermal model for aluminium at 5 GHz

The Q-factor seems to give a more reasonable result, with a maximum for Q_s around 1500. This gives the optimal thickness for Aluminium contacts at approximately $t = 50\ nm$. We can see that Q_p, which is the Q-factor for the amplitude of the impedance, becomes quite high for the thicker contact thicknesses. I have not been able to investigate this effect due to the lack of time, but it seems to be a very interesting effect.

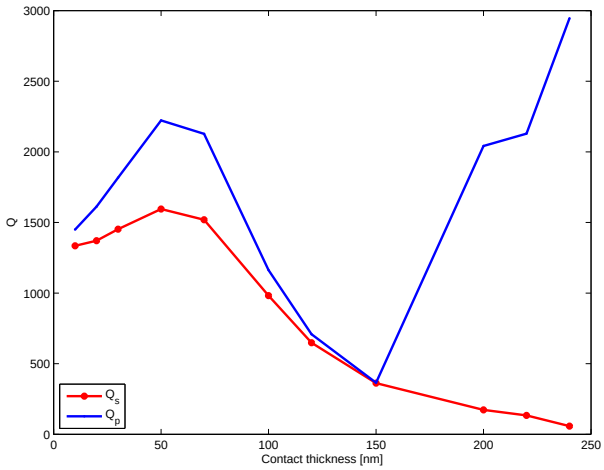

Figure 5.15: Q_s and Q_p for aluminium at 5 GHz

We can see in *Figure 5.16* that the figure of merit for the Aluminium contacts on the FBAR is around 100, which seems to be a realistic result.

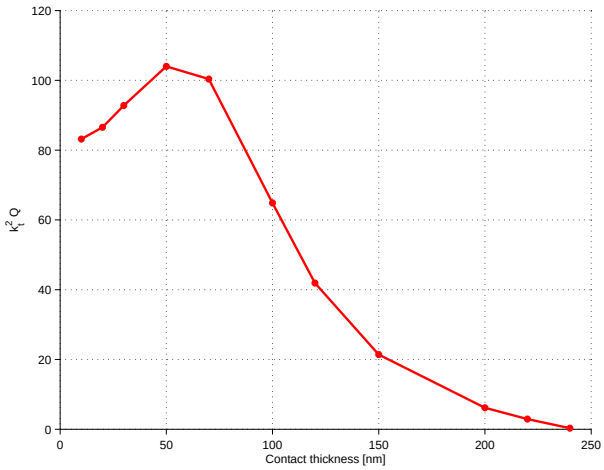

Figure 5.16: Figure of merit for aluminium at 5 GHz

5.6 Future work

This thesis has considered a very simplified FBAR structure, using only longitudinal vibrations and a freely vibrating structure. It would be interesting to expand this model to include more vibration modes, especially the lateral vibration mode, which can contribute quite a bit to the loss of performance in the FBAR. Even on this simple structure investigated here, the calculations becomes quite large, and in order to perform even further analysis, the use of more sophisticated methods needed.

A logical progression would be to investigate the device with Finite Element (FEM) software, to compare the results to the Matlab model. With FEM software, both 2D and 3D models of the same structure could provide more valuable knowledge in order to quantify the thermoelastic losses in the contacts of the FBAR.

Further on, the other loss effects could be modeled in the FEM-model in order to approach the performance of a real device, which has considerable lower performance than the device investigated in this thesis.

5.7 Conclusion

An analytical model for an FBAR structure, including and not including thermal effects has been modeled. Different materials has been tested in the model to see if the performance is affected when the thermal effects are included.

The models seems to fit well with earlier work being done to similar structures. Most of the previous work has been done on real devices, which is not as idealized as this model. The real devices will include more loss effects, giving lower performance than the idealized models in this thesis. For the very thin layers, either contact layer og piezoelectric layer, the Q-factor increases noticeably. The main focus has been to compare the midrange contact thicknesses, $100 - 200$ *nm*, which is probably a more realistic thickness to use in a real device. Compared to other work done, the results seems to match pretty good regarding the relative performance differences between the materials.

The exact influence of the thermal effects has been difficult to pinpoint. The most noticeable effect has been the lowering of the resonance and antiresonance frequency for the thermal model compared to the non-thermal model. This could be due to a lowering of the stiffness of the system, when the thermal effects are introduced. It seems that the largest difference in resonance and antiresonance frequencies has been around the midrange contact thicknesses.

Comparing the effective coupling for the two models, there hasn't been any particular influence by the thermal effects other than the coupling. It has been a little bit higher for most of the thicknesses for the thermal model, apart from the case where the contact thicknesses are extremely large compared to the piezoelectric layer. This can be due to the piezoelectric layer having much less influence on the performance on these small thicknesses.

Update Due to the unfortunate events of finding a small error in the code, which resulted in large errors in the results, I haven't been able to recalculate the results for the different materials. An example for Aluminium has been done, and it shows much better results. The Q-factor has a reasonable size for FBAR, and the effective coupling coefficient is practically identical to the non-thermal model which shows confirms that the thermal model gives good results compared to the much simpler non-thermal model.

Bibliography

[1] G. Askar Altay and M. Cengiz Dokmeci. Fundamental variational equations of discontinuous thermopiezoelectric fields. *International Journal of Engineering Science*, 34(7): 769–782, May 1996. ISSN 0020-7225.

[2] NSM Archive. Aluminium nitride (aln). URL `http://www.ioffe.ru/SVA/NSM/Semicond/AlN/index.html`.

[3] Bertram A. Auld. *Acoustic Fields and Waves in Solids*, volume 2. Krieger Publishing Company, 1990.

[4] Ron Lifshitz and M. L. ther Roukes. Thermoelastic damping in micro- and nanomechanical systems. *Phys. Rev. B*, 61(8):5600–5609, February 2000.

[5] W. P. Mason. *Piezoelectric Crystals and Their Application to Ultrasonics*. Van Nostrand, New Jersey, 1950.

[6] A.S. Nowick and B.S. Berry. *Anelastic Relaxation in Crystalline Solids*, volume 1 of *Materials Science Series*. Academic Press, New York, U.S.A., 1972.

[7] J. F. Nye. *Physical Properties of Crystals - Their Representation by Tensors and Matrices*. Oxford University Press, 1960.

[8] Sairam Prabhakar and Srikar Vengallatore. Thermoelastic damping in bilayered micromechanical beam resonators. *Journal of Micromechanics and Microengineering*, 17:532–538, February 2007.

[9] Harry F. Tiersten. *Linear piezoelectric plate vibrations : elements of the linear theory of piezoelectricity and the vibrations of piezoelectric plates*. Plenum Press, New York, 1969.

[10] M. Ueda, T. Nishihara, J. Tsutsumi, S. Taniguchi, T. Yokoyama, S. Inoue, T. Miyashita, and Y. Satoh. High-q resonators using fbar/saw technology and their applications. *Microwave Symposium Digest, 2005 IEEE MTT-S International*, pages 4 pp.–, June 2005. ISSN 01490-645X. doi: 10.1109/MWSYM.2005.1516561.

[11] Keiichi Umeda, Hideki Kawamura, Masaki Takeuchi, and Yukio Yoshino. Characteristics of an aln-based bulk acoustic wave resonator in the super high frequency range. *Vacuum*, 83(3):672–674, 2008.

[12] Magne Vestrheim. Lecture notes in phys272 - acoustic transducers, 2008.

[13] WebElements. Webelements: the periodic table on the web. URL `http://www.webelements.com`.

[14] T. Yokoyama, T. Nishihara, S. Taniguchi, M. Iwaki, Y. Satoh, M. Ueda, and T. Miyashita. New electrode material for low-loss and high-q fbar filters. *Ultrasonics Symposium, 2004 IEEE*, 1:429–432, August 2004. doi: 10.1109/ULTSYM.2004.1417754.

[15] Clarence Zener. *Elasticity and Anelasticity of Metals*. University of Chicago Press, Chicago, IL., 1948.

[16] Shu-Ang Zhou. *Electrodynamics of Solids and Microwave Superconductivity*. John Wiley & Sons, Inc., 1999.